PASSIVELY ACTUATED VIBRATION TO DECREASE MEMBRANE FOULING RATE FOR CENTRIFUGAL REVERSE OSMOSIS

A Thesis

by

MATTHEW AARON MARTINEZ

Submitted to the Office of Graduate and Professional Studies of
Texas A&M University
in partial fulfillment of the requirements for the degree of

MASTER OF SCIENCE

Chair of Committee,	Alan Palazzolo
Committee Members,	Michael Pate
	Peter Keating
Head of Department,	Andreas Polycarpou

August 2018

Major Subject: Mechanical Engineering

ABSTRACT

A novel method of shaking a CRO membrane was designed. This method, called the Plug and Pipe method, was simulated to determine how well it would work in a full CRO system. This was done by a series of simulations. First, the geometry was meshed and a CFX simulation was performed. This would be used to find the water velocity at discrete points along the radial direction of the orifice. These discrete velocities were then put into a curve fitting program, MATLAB's $cftool$ which provided a velocity distribution across the orifice. This velocity distribution was then integrated and to find the flow requirements and water jet force, F_{jet}. F_{jet} was found to depend in large part on the orifice size, while other variations, such as Pipe length and diameter, had little to no effect. F_{jet} varied from 27.13 N to 94.64 N, based on orifice size. This water jet force was then included in a dynamic model, which was created to describe the nonlinear equation of motion of the shaker. This dynamic model had two parts. The first was the script into which the characteristics of the system were put, called osc_model, while the second was the function which held the nonlinear forcing functions for the water jet and wall interactions. The simulated shaker was designed based on a test size membrane of 28 kg. It was determined that the shaker would be capable of providing the proper dynamic characteristics based on previous work, which were a $1\mathrm{mm}$ amplitude of vibration at 20 Hz.

Another model was created to show the amount of mass that could be shaken by a full shaker based on the orifice size and wall stiffness. The orifice diameter was varied from 0.16 in to 0.5 in, while the wall stiffness varied from $10^5\mathrm{N/m}$ to $10^8\mathrm{N/m}$. It was found that, as stiffness approached 10^8 $\mathrm{N/m}$, the amount of mass that could be shaken began to plateau, meaning that this was the value at which the wall began to act rigidly for this system. The flow requirements were provided for each orifice size as well, and it was determined that any orifice diameter above 0.25 in would have excessive flow requirements and would limit a CRO rig's ability to purify water.

An experimental rig was built based on the specifications set out in the simulations as well. A high pressure gear pump was used to bring the water up to osmotic pressure, about 800 psi. This

high pressure water went into the shaker. It was intended that once the shaker showed vibration, adjustments would be made to achieve the 1 mm and 20 Hz vibration set by previous work. Upon final installation, however, there were misalignment problems between the shaft and the linear bearings, which prevented the shaker from vibrating at all.

DEDICATION

To my parents, without whom none of this would be possible.

ACKNOWLEDGMENTS

I would like to thank my advisor, professor Alan Palazzolo, and my committee members, Professors Pate and Keating. I would also like to thank Erwin Thomas and the rest of the Vibration Lab at Texas A&M University for their support. I would also like to thank the Texas A&M University System Louis Stokes Alliance for Minority Participation as well as the National Science Foundation for the Bridge to the Doctorate Fellowship which supported me more than just financially during my Master's degree.

CONTRIBUTORS AND FUNDING SOURCES

Contributors

This work was supported by a thesis committee consisting of Professor Alan Palazzolo [advisor] and Professor Michael Pate of the Department of Mechanical Engineering and Professor Peter Keating of the Department of Civil Engineering.

All other work conducted for the thesis was completed by the student independently.

Funding Sources

Graduate study was supported by a fellowship from Texas A&M University System Louis Stokes Alliance for Minority Participation NSF Bridge to the Doctorate Fellowship, along with the Texas A&M Engineering Experiment Station.

NOMENCLATURE

RO	Reverse Osmosis
CRO	Centrifugal Reverse Osmosis
Pipe	The portion of the shaker unit design that acts as the housing, inside of which the water and Plug are contained
Plug	The portion of the shaker unit design that alternately plugs the orifices on either side of the Pipe
XXS	Double Extra Strong (referring to steel pipe)
FFT	Fast Fourier Transform
FOFC	Fully-Open, Fully-Closed
OBE	Open on Both Ends
DAQ	Data Acquisition
RMS	Root Mean Square

TABLE OF CONTENTS

Page

LIST OF FIGURES

FIGURE Page

LIST OF TABLES

TABLE Page

1. INTRODUCTION

1.1 Global Water Scarcity

Water scarcity is a global epidemic that is increasing in both breadth and severity. 38% of the world's population lives in a place with water scarcity due to either environmental or economical factors [1], and the amount of people affected is constantly increasing. This scarcity will only by exacerbated as the world's population continues to grow. According to the United Nations Human Development Report [2], water demand tends to grow at a rate of twice the population growth, which is already projected to reach 9.7 Billion by 2050.

Water scarcity brings with it a host of other problems as well. Those that have no access to clean water are forced to drink from tainted sources, causing serious and long-lasting health issues, as well as a low life expectancy and quality of life. People in these areas are also often forced to spend hours walking to the nearest source of clean water, which may be miles away. This burden, which often falls on children (usually young girls), leaves them susceptible to attack on the road and prevents them from going to school. Without easily accessible clean water, it is extremely difficult for a struggling region to advance.

It is for the reasons listed above that provision of access to clean water is considered by the National Academy of Engineers to be one of the fourteen Grand Engineering Challenges of the 21st century.

It was estimated by the Center for International Earth Science Information Network at Columbia University that the total amount of people living within 100km of the coast (or with <10km elevation above and direct access to the coast. See Figure 1.2) is about 40% of the world's population [3]. The breakdown by country can be seen in Figure 1.1. This means that any progress made to increase clean water accessibility to areas near the coast has the potential to affect a large portion of the world. Thus, this project was focused on advancing the prospects of low-cost seawater desalination.

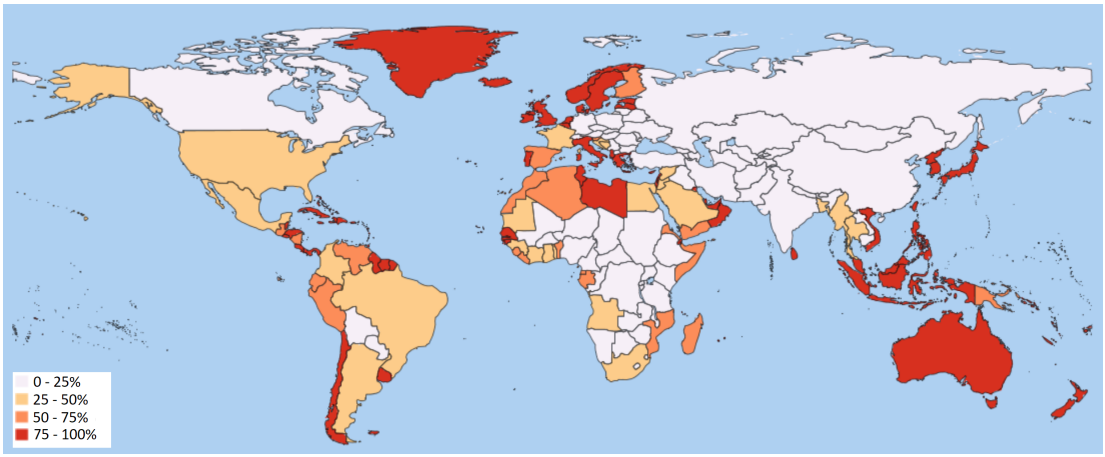

Figure 1.1: Percentage of population living within 100km of the coast by country (based on 2010 estimates). Reprinted from National Aggregates of Geospatial Data Collection [4]

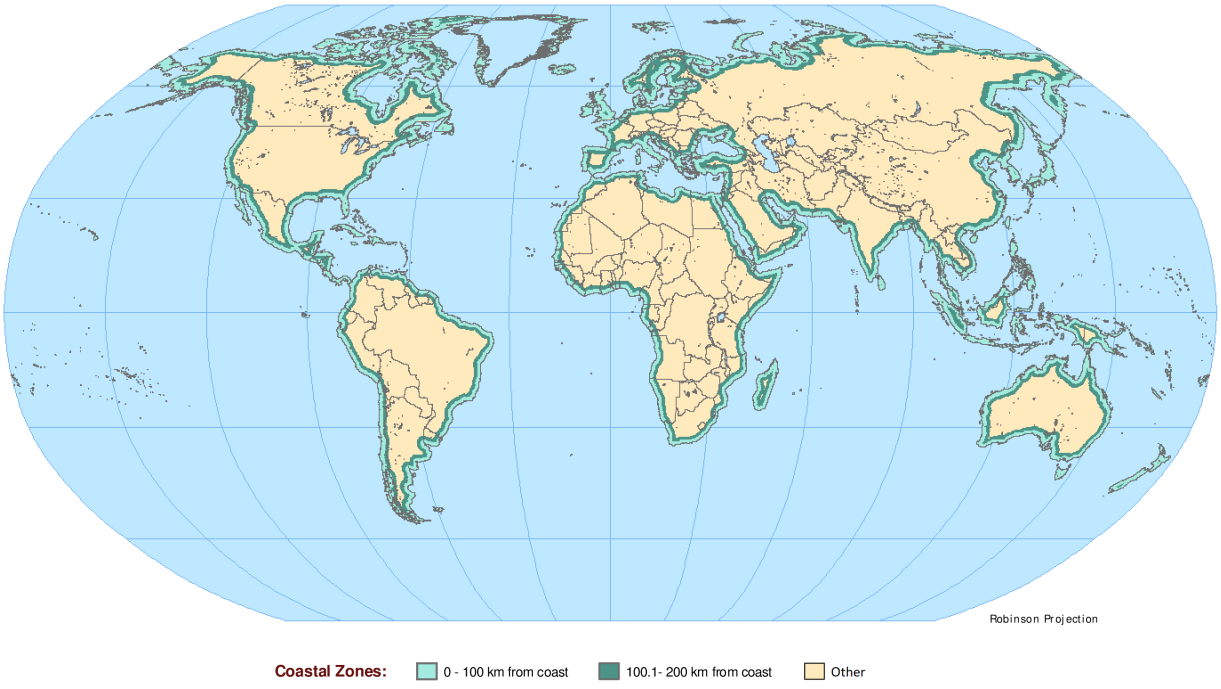

Figure 1.2: Visual of the 100km band. Reprinted from National Aggregates of Geospatial Data Collection [5]

1.2 Reverse Osmosis and Desalination

Seawater desalination has been around for centuries in the form of distillation, with evidence to suggest the use of basic solar stills in the 16th century Middle East. The relatively low output for large energy inputs has kept distillation from being properly scalable for large cities and developments, while personal distillation units have proven to be low yield and cost prohibitive. For decades now, the most common method of large-scale seawater desalination has been Reverse Osmosis.

Reverse Osmosis (RO) commonly uses large positive displacement pumps to push feed water (brine) to a high pressure (about 800 psi) which will force some of the brine through the membrane (the system can be designed for a certain recovery rate), while the rest leaves as high pressure brine. A simplified process flow diagram (PFD) can be seen below in Figure 1.3. This system runs into several problems, which cause maintenance costs to remain high.

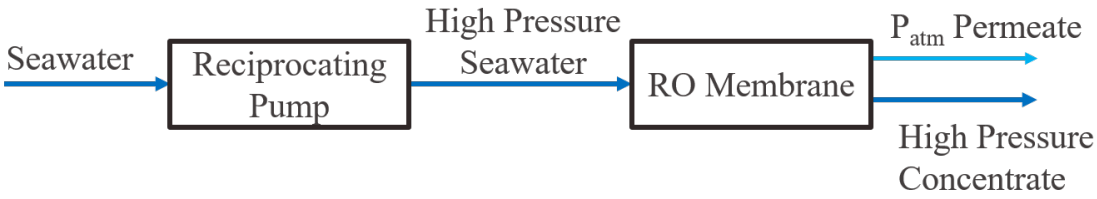

Figure 1.3: Simplified PFD of a traditional reverse osmosis system

The first problem is the high pressure concentrate, or the brine that does not pass through the membrane. The concentrate is energized and must be de-energized in order to be recycled back into the system. Here is an inherent waste of energy. Either the brine is simply depressurized and recycled back, wasting all of the concentrate's energy, or it is put through a turbine to to generate power, as is found in a cogeneration unit. However, even with cogeneration, there is inherent loss due to turbine efficiency. Additionally, the corrosive nature of high pressure brine lead to frequent

outages for turbine replacement.

Oftentimes, RO plants will try to reduce this loss of energy as much as possible by keeping their recovery rates high. This means that a higher percentage of the feed is pushed through the membrane to become clean water. However, by increasing the recovery rate, the fouling rate of the membrane will also increase, leading to the need for more frequent membrane replacement. It is estimated that membrane replacement is about 4% of the total cost of RO unit upkeep, but this number increases significantly as the recovery rate increases, which is why most units keep relatively low recovery rates and make use of cogeneration.

Another common problem with RO systems is the reliability of the reciprocating pumps used to push the feed water up to the osmotic pressure. The reciprocating seal faces have a relatively high rate of failure, leading to regular pump outages to replace seals. The failure rate is due to the fact that this configuration forces the seals to hold high pressure at the point of sealing, so even if the rubbing speed is slow, there is a higher rate of failure [6]. This is one of the main reasons that the estimated run time of a unit is only 7884 hours per year, or less than 90% [7]. This is below the commonly accepted minimum requirement of 8000 hours per year to be considered a continuous operation plant. If RO is to be a viable source of water provision for large cities, then it is necessary for the process to be reliable enough to run continuously.

1.3 Centrifugal Reverse Osmosis

In response to these problems, it was proposed by Wild et al. that a reinvention of the RO process would be beneficial. Thus, they presented the Centrifugal Reverse Osmosis (CRO) unit [8]. This unit had the same basic principles as traditional RO, but the configuration of the components was entirely changed. Instead of using reciprocating pumps to push the feed water to the osmotic pressure, the water flows through a centrifuge. As the water is pushed to the outside of the centrifuge, the pressure of the water increases to the required 800 psi. Additionally, the membrane is placed near the outside of the centrifuge, so that the pressure difference on either side of the membrane is enough to drive the feed water through it. A simplified PFD of this process is found below in Figure 1.4

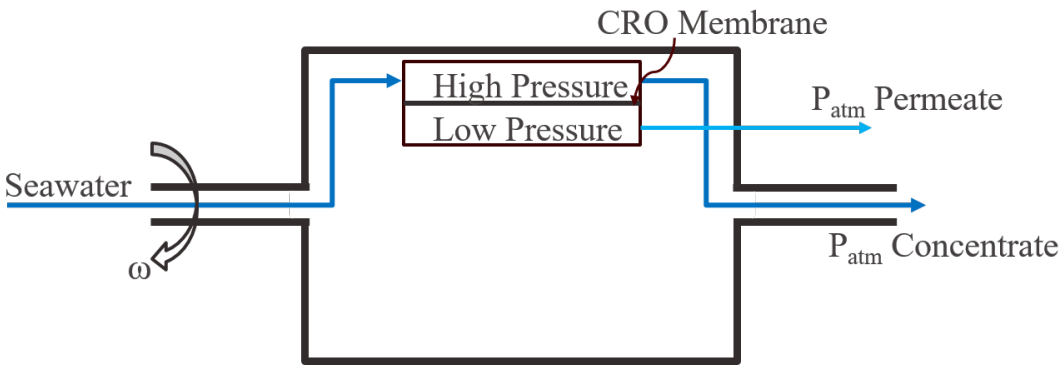

Figure 1.4: Simplified PFD of a Centrifugal Reverse Osmosis system

This design corrected many of the problems with traditional RO. By using a centrifuge, the reciprocating seal faces were foregone entirely and replaced by rotating seal faces, which are far less prone to failure. This is due to the fact that this configuration allows for lower pressures at the seal faces, which increases their longevity despite the higher rubbing speed [6]. Additionally, there was no unused pressurized water, as the concentrate inherently will be brought back to the inlet pressure, per the conservation of angular momentum. This is perhaps the biggest point of energy savings that CRO provides.

Additionally, this design allows the system to run at low recovery rates with no penalty. As discussed above, with traditional RO there was a need to minimize wasted energy that drove the recovery rates to be high. Correction for this has in some cases led to high membrane costs and regular outages for membrane replacement. However, since there is no wasted energy on the concentrate, there is no penalty (other than a lower output) for keeping recovery rates low. This allows the system to increase the amount of time between membrane replacements, which not only decreases membrane cost, but also decreases required downtime for the CRO system.

CRO is still in early stages of development. Since centrifuge size is limited by cost and space, the overall output of a single CRO unit seems to be less than that of a traditional RO unit. However, it is the goal of CRO to minimize energy requirements enough to overcome the production limitations of a single unit and become a more economical form of seawater desalination.

1.4 Axial Vibrations and CRO

It is widely accepted that transverse flow across membranes was preferable to normal flow in order to keep shear rates high and minimize concentration polarization. This phenomenon was studied extensively in the mid-to-late twentieth century [9, 10, 11]. In the early 1990's, however, it was discovered that concentration polarization could be mitigated even further if the membrane over which the liquid flowed was vibrating. This style of vibrating membrane separation came to be known as Vibratory Shear Enhanced Processing (VSEP) [12]. This decrease in concentration polarization is believed to be caused by the complex flow patterns that are introduced with vibration. The vortical flow constantly washes salt buildup from the membrane, greatly reducing the concentration polarization which plagues membranes in general membrane filtration. This discovery led to the adoption of VSEP filtration in a variety of fields as its effects on varying solvents and configurations (with both organic and inorganic solutes) were studied [13, 14, 15, 16].

Shi et al. then brought VSEP filtration into the field of RO desalination. Here, VSEP filtration continued to bring decreased concentration polarization and increased membrane longevity [17, 18].

More recently, Su et al. compared the results of multiple shaking frequencies on the output of a RO desalination unit over time. They found that the permeate flux was significantly higher with the presence of vibration, and that increasing shaking frequency led to increased permeate flux [19]. These simulations and experiments were performed with a vibration amplitude of 1 mm and varying frequencies. The shaking done in this study was driven by linear motors. Applying comparable motors to a full CRO system, however, would increase the energy required by 25%. Because low energy requirement is one of the major benefits of CRO, a passive method of shaking was pursued.

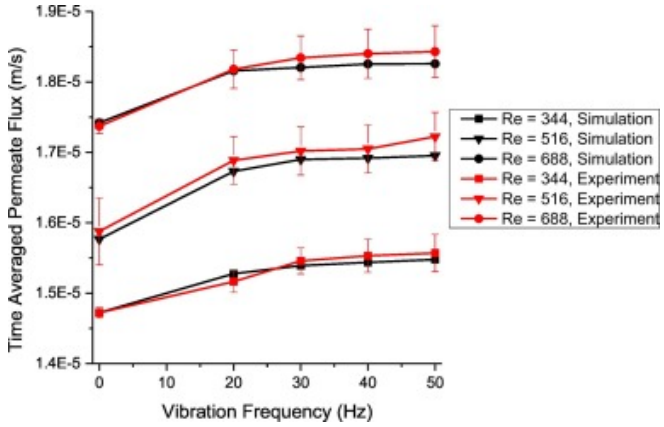

Figure 1.5: Numerical and experimental results showing permeate flux vs shaking frequency at varioud Reynold's numbers. Reprinted from "Concentration polarization and permeate flux variation in a vibration enhanced reverse osmosis membrane module" by Xu Su et al., 2018, *Desalination, 433*, p.75-88

One note before the continuation of this document: The terms "energized water" and "pressurized water" are used interchangeably throughout. This is because the pressure provided by the centrifuge is the only usable source of energy in the water.

2. METHODS

2.1 Design

Because the project was focused on a passively actuated vibration system, there were limited options an energy source to drive the vibration. The design objectives for this device follow. The device must:

1. Be capable of shaking a membrane assembly at a prescribed amplitude and frequency
2. Be driven by energy already present in the system
3. Not interfere with desalination
4. Be capable of fitting inside the centrifuge housing
5. Be able to provide 1D vibration in a rotating frame of reference

Objectives 1 and 2 are simply restatements of the initial problem: to design a passive shaking mechanism for a prescribed set of parameters. Objective 3 is where most of the process of narrowing down potential candidates occurred. When designing a passive shaker, it is important that the amount of energy required for shaking not interfere with the process of desalination. Additionally, Objectives 4 and 5 severely limited the mechanism of movement used, as the device was required to be small and effective in the presence of radial acceleration.

It was decided that, as long as the flow required was minimal compared to the overall flow through the centrifuge, pressurized water would be a good energy source for the shaker. Since the goal of the centrifuge is to push water through the membrane, this device must be designed to take as little flow away from that goal as possible, or it would conflict with objective 3. It was also desired that the shaker be capable of fitting inside of the housing of a centrifuge so that it would be able to shake just the membrane and therefore decrease the amount of energy, and subsequently

the amount of diverted flow, required. Due to these limitations, the amplitude and frequency of shaking were decided to be the lowest of those tested by Su et al. [19], or $1\ \mathrm{mm}$ at $20\ \mathrm{Hz}$.

Several different methods of fluid-driven vibration were considered and split into two main categories: direct and indirect drives. Direct drive mechanisms are those where the motion of the fluid itself causes vibration in an object. This category includes devices such as the rotary water sprinkler, or the oscillatory flow valve (though these valves are generally for gases). The benefit of these types of mechanisms is that they tend to be mechanically simple, which allows them to have high reliability. Their downside, however is that the flow required to run these devices is quite high compared to the force they provide. The simplicity of these devices requires that the flow be diverted in such a way that only a fraction of the fluid ends up contributing to the desired vibration direction.

Indirect drive mechanisms are those that take an energized fluid and use a device (usually a turbine of some sort) to de-energize the fluid and transfer that energy to another mechanism, which in this case would be a shaker. Examples of these devices include the steam turbine and the water wheel. These kinds of devices are useful for creating rotational motion, and tend to have lower flow requirements than direct drive. However, the drawbacks of these mechanisms include low energy yield for the water wheel (limited by the velocity of the water) and blade degradation for any traditional turbine due to the corrosive nature of brine.

Due to the major limitations of each of the methods enumerated above, a novel method of water-driven vibration was pursued, which will be referred to as the Plug-and-Pipe method. A simple schematic of the shaker is shown in Figure 2.1. It has two major components. The first is the solid dumbbell shaped object in the center, which serves to alternately close the orifice at either side of the shaker. This part will be hereafter referred to as the Plug. The second is the housing for the shaker, inside which the Plug sits. This second part has the orifices on either side and will be hereafter referred to as the pipe.

This Plug-and-Pipe method has an inlet at the top, where the high pressure water will enter the pipe. A detailed description of the Plug-and-Pipe method, as shown in Figure 2.1, follows. The

Pipe will be filled with this high pressure water, which will naturally want to flow out of the orifices to the low pressure area outside the Pipe. The Plug will start on one side of the Pipe. Since that orifice will be plugged, the water will flow out the other orifice, creating a water jet that pushed the whole assembly the opposite way (top). Then, eventually the Plug will hit a wall, opening both orifices and creating a net zero force on the assembly. The Pipe, however, will continue to move due to its momentum (middle) until it runs into the Plug on the opposite orifice. Then, a new water jet is created, pushing the assembly the opposite way (bottom). This process then repeats indefinitely.

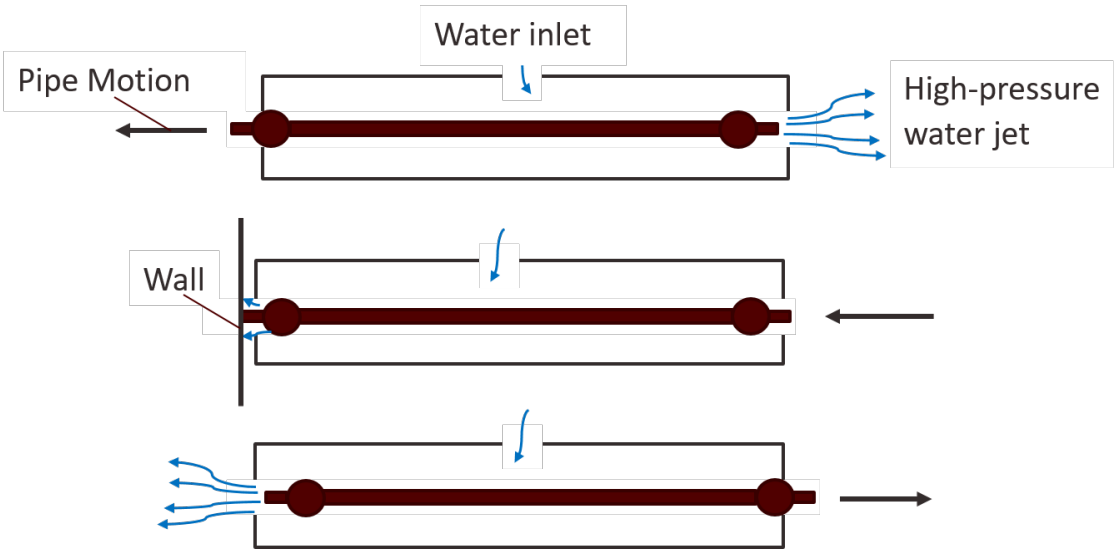

Figure 2.1: The shaker being pushed left by the water jet (top), preparing to switch directions as the Pipe catches up to the plug (middle) and then being pushed back to the right by the opposite water jet (bottom)

When creating the full model for the shaker, one of the key design considerations was to maximize the use of Commercial Off-The-Shelf (COTS) parts. Other than the Pipe (a modified 1.5 inch XXS steel pipe), the end caps and end plates (modified steel plates), and the Plug (machined from rolled stainless steel), all of the parts are COTS and available from most large manufacturers.

2.2 Simulation

In order to describe both the means by which the shaker/membrane unit is driven (further discussed in Section 2.1) and its motion, the math was derived from two disciplines: Fluid Mechanics, and System Dynamics. The calculations are straightforward and in Sections 2.2.1 and 2.2.2.

As for the modeling of the device itself, a detailed 3D model (off of which the CFX simulation geometries were based) was created using SolidWorks. The models for individual parts, as well as the overall assembly can be seen below:

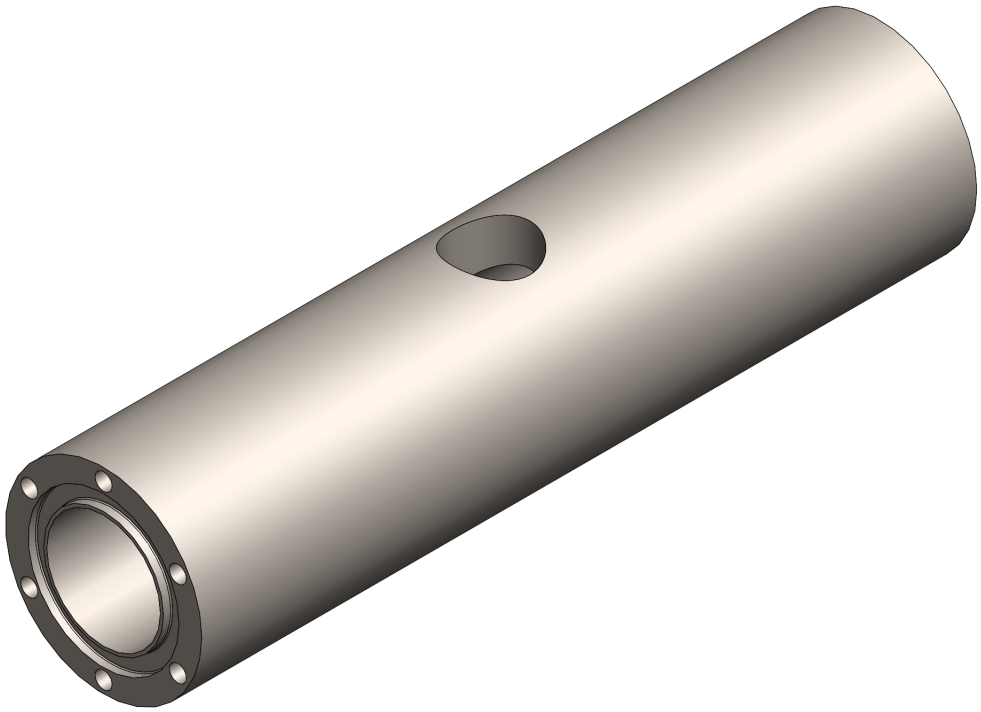

Figure 2.2: SolidWorks model of the Pipe

Figure 2.3: SolidWorks model of the Plug

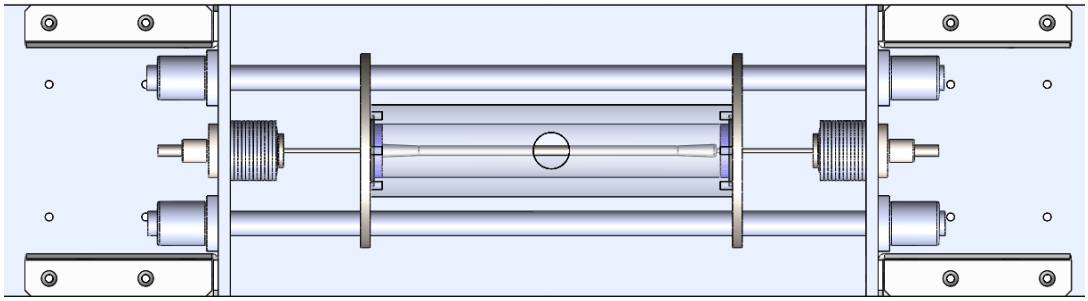

Figure 2.4: Solidworks model of the overall assembly, from the top

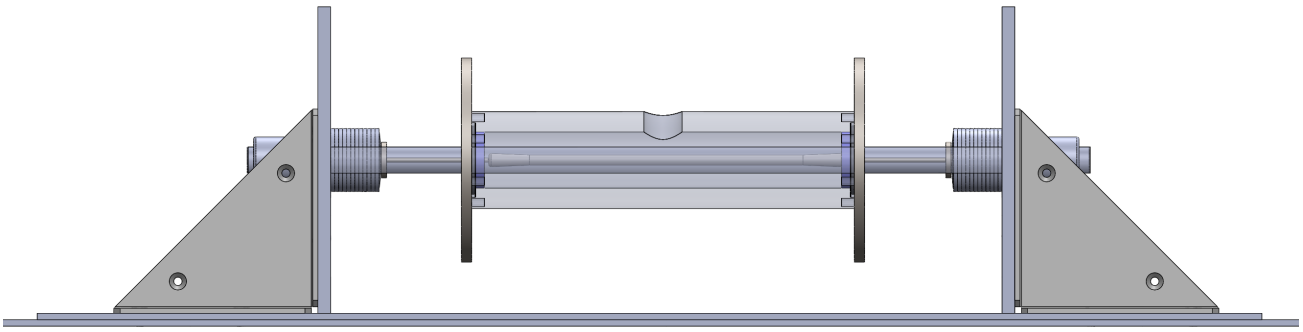

Figure 2.5: SolidWorks model of the overall assembly, from the side

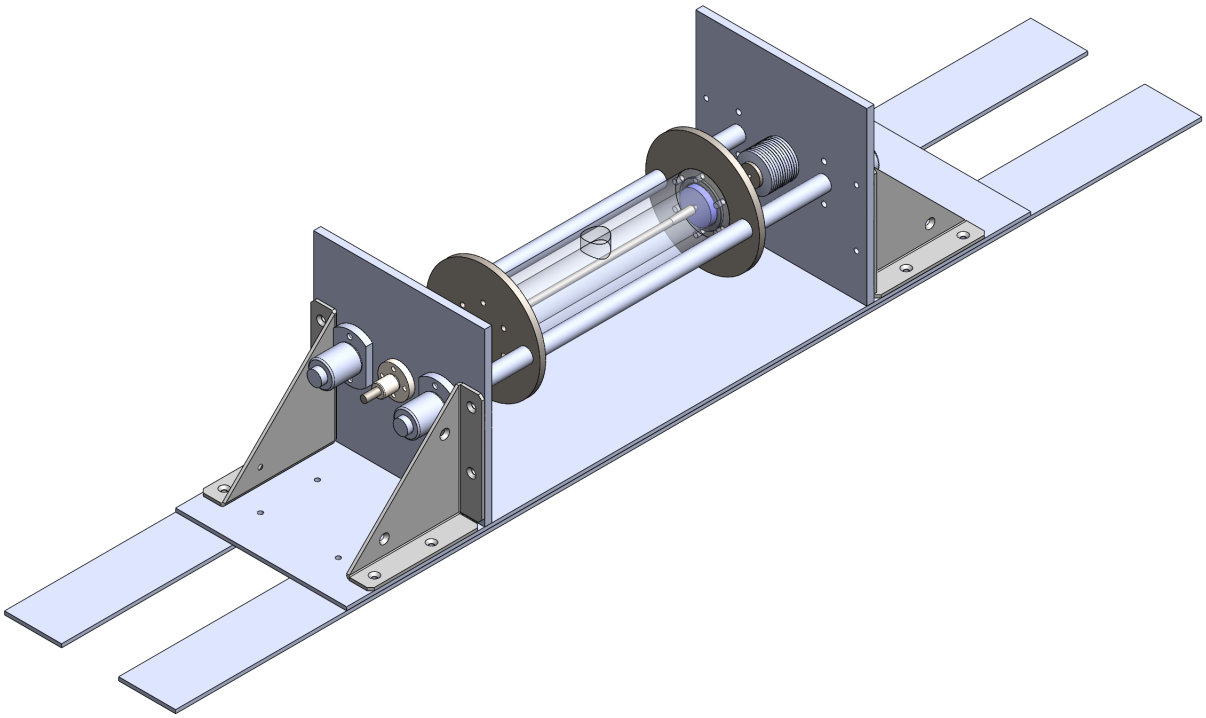

Figure 2.6: Isometric view of the overall assembly

This shaker was designed to shake the mass of a small-scale centrifuge membrane. The mass was based on a membrane unit set up in the lab, which came in at 28 kg. The dimensions from

these models were used to create engineering drawings, the geometries for the CFX simulations, and some of the parameters for the MATLAB simulations. As adjustments were made to adjust the dynamics of the system, the SolidWorks models were also adjusted. The overall rig components and dimensions can be found in Figures 2.7 and 2.8, as well as Table 2.1. Individual drawings of each of the machined components are found in Appendix A.

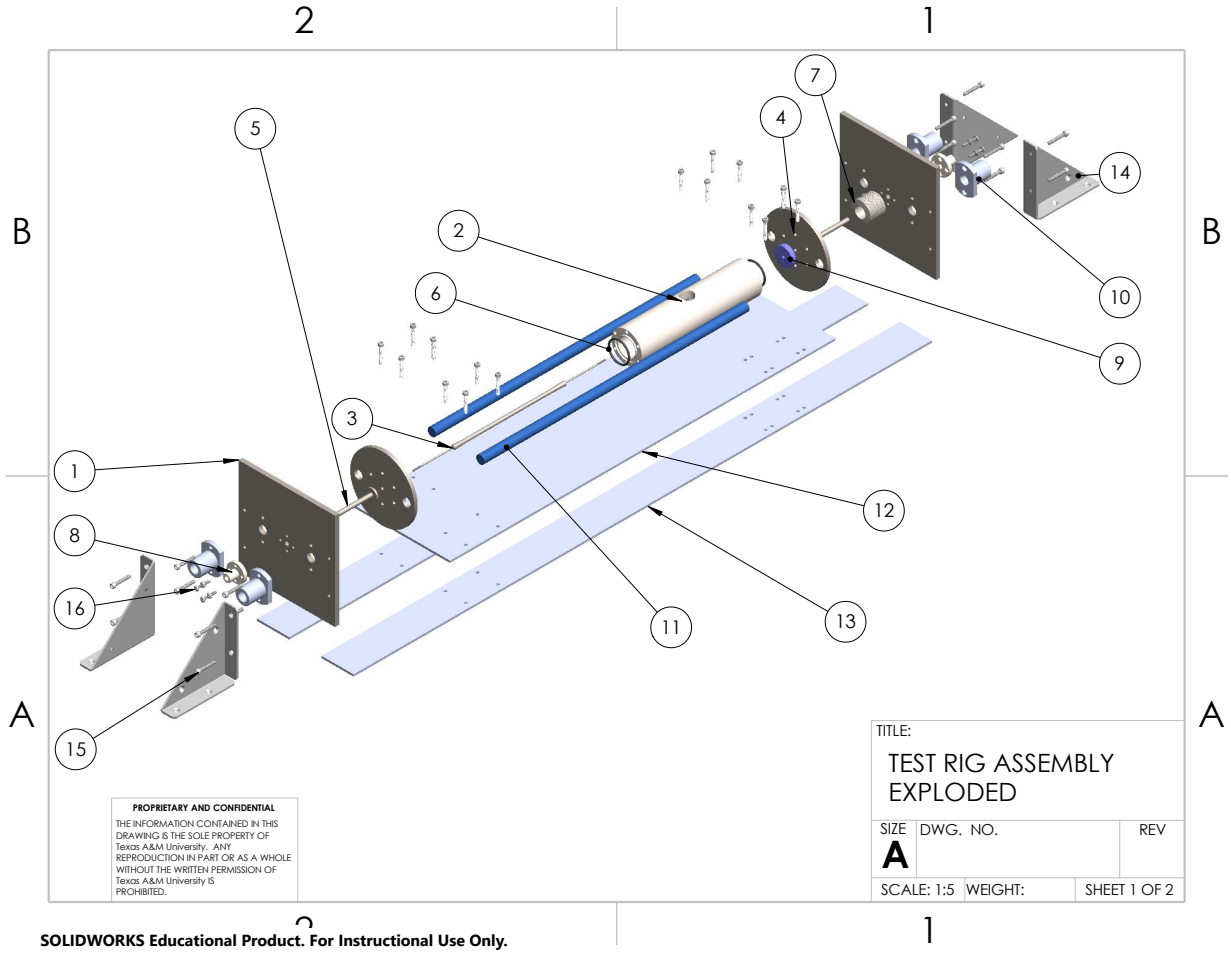

Figure 2.7: Exploded view of the overall assembly.

Table 2.1: Bill of materials for the overall assembly

Item Number	Part Name	Description	Qty.
1	Test Rig End Plate	See Appendix A	2
2	Test Rig PV (aka Pipe)	See Appendix A	1
3	Test Rig Plug	See Appendix A	1
4	Test Rig End Cap	See Appendix A	2
5	Test Rig Plug Cap	See Appendix A	2
6	O-ring	Highly Saturated Nitrile O-ring for 1-3/16in ID	2
7	Belleville Washers	Chrome vanadium steel. 16.3mm minimum ID, 2mm thick	24
8	6mm Linear Bearing	52100 bearing steel, round flange	2
9	Sorbothane Disc	Neoprene disc to aid with seal at end caps	2
10	13mm Linear Bearing	52100 bearing steel, compact flange	4
11	13mm Shaf	440C stainless steel, 450mm long	2
12	Shaker Base	See Appendix A	1
13	Shaker Support Beam	See Appendix A	2
14	Support flange	Inside corner support bracket with 4in sides	4
15	1in Socket Screws	8-32 316 stainless steel socket screws. Corresponding nuts included, but not shown	32
16	10mm Slot Screws	M3.5x0.6 316 stainless steel screws. No corresponding nuts due to internal threading of end plate	8

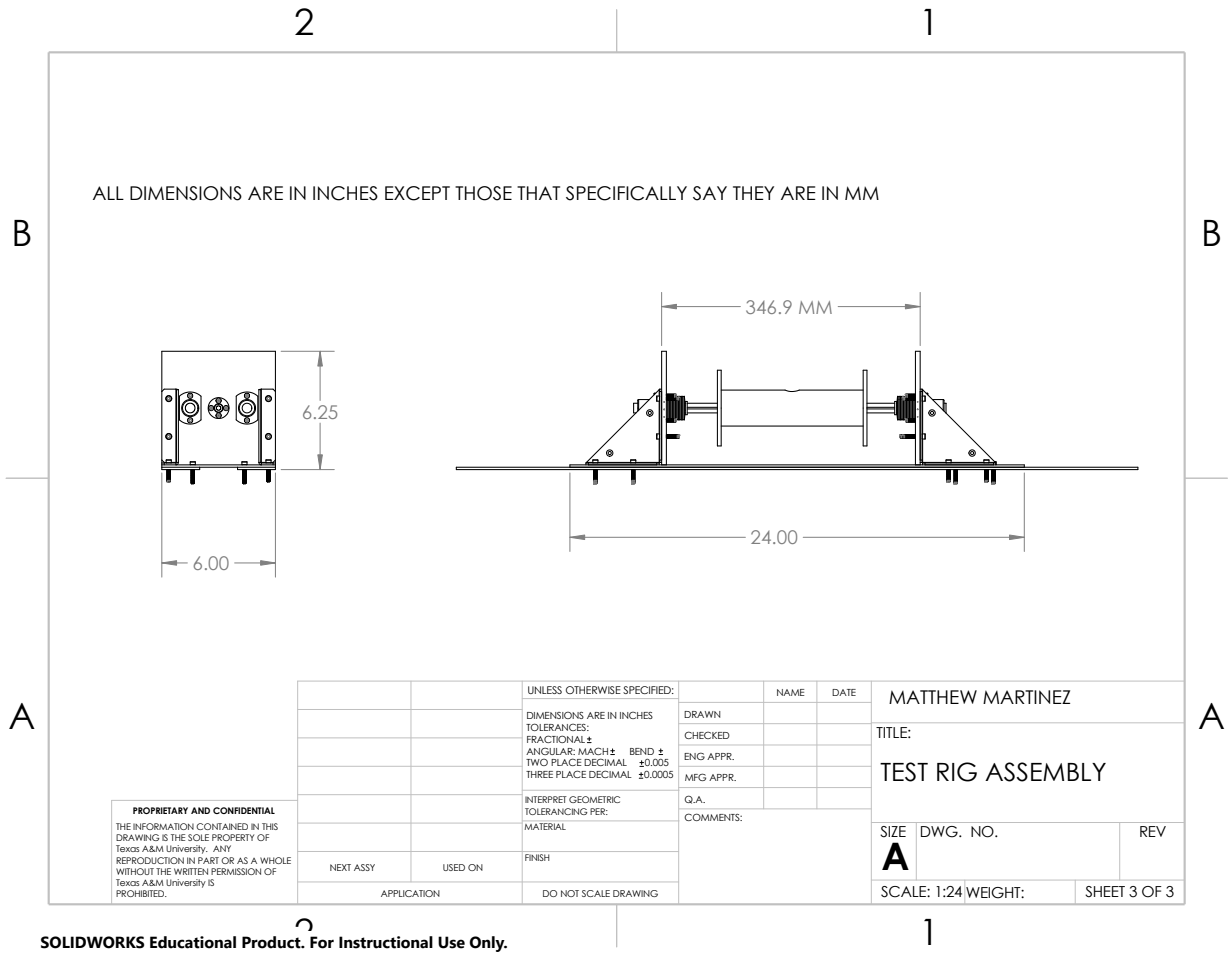

Figure 2.8: Overall measurements of the test rig assembly

It is important to note that the models shown above are for the test version of the shaker. In order for the shaker to be implemented in a real CRO unit, there would be a bigger focus on minimizing the footprint of the device (decreasing the sizes of the end plates, possibly reducing the length, etc.).

One key design feature of the rig is that the Plug caps have 1 mm of clearance between them and the washers which stick out from the end plates. The washers serve to provide the ability to adjust the shaking amplitude for future experiments. In addition to this 1 mm clearance, there needs to be 1mm of clearance between the Plug and the sealing face of the end plates, which are within the Pipe. These two combined clearances are what allow the 2 mm of total stroke, which

translates to a $1\ \mathrm{mm}$ amplitude of vibration.

2.2.1 Fluid Mechanics

The basis for the CFD model and force calculations are provided in this section.

The F_{jet} contribution to Equation 2.8 came from a series of ANSYS CFX Simulations. The geometry to be used for the simulations, which was based on the SolidWorks model, can be seen below. This simplified geometry was created solely for the CFX simulations. The flow area is created from the subtraction of two geometries, which was performed in the ANSYS Design Modeler. The Plug body was subtracted from the Pipe body (and the plug body was not preserved), meaning that there is no fluid flow through the Plug. The Pipe includes a protrusion so that the velocity of the fluid as it leaves the orifice would be properly modeled. The geometry used for the mesher and subsequent simulations can be seen in Figure 2.9. As explained in Section 2.1, the Plug was designed to block part of the orifice even when fully open, so that the walls would be able to control the Plug motion separately from the Pipe motion. The Plug geometry was modeled accordingly.

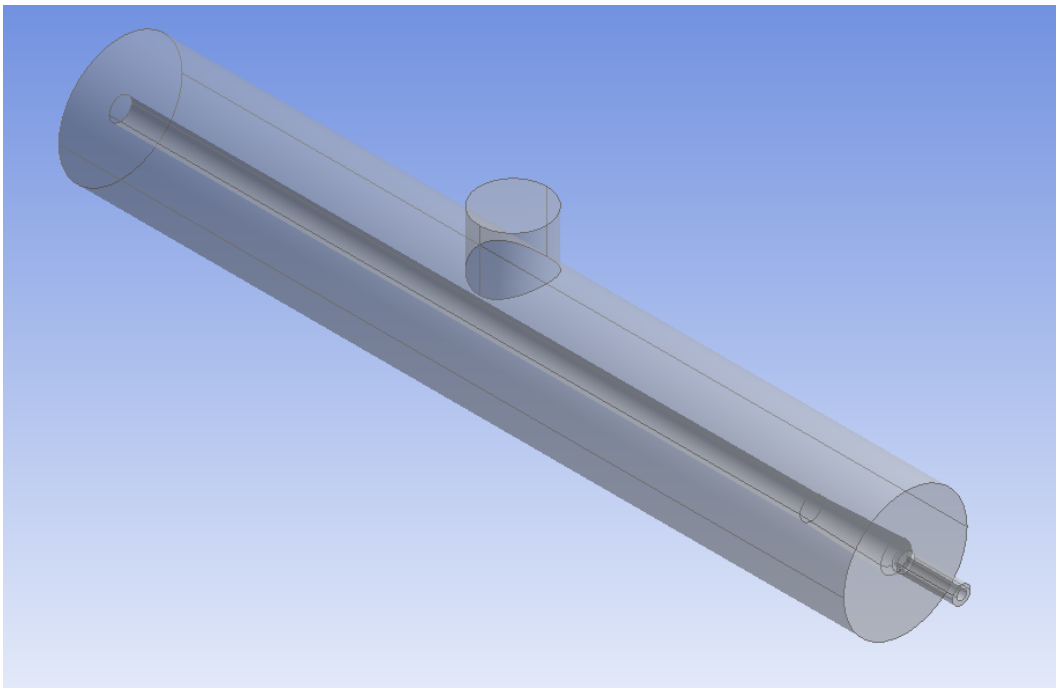

Figure 2.9: Fluid simulation area for the CFX Simulations.

Next, ANSYS Meshing was used to generate a mesh for the analysis. The mesh was tetrahedral with a coarse relevance center and a sizing function based on proximity to other faces or edges. The maximum face size was set to $1\mathrm{mm}$. Since there were no small features to consider, mesh defeaturing was allowable, and the defeature size set to $0.8\mu\mathrm{m}$. The transition rate was kept at "slow," and the growth rate and max tet size were left to their defaults (1.20 and $1\mathrm{mm}$, respectively). The minimum size based on proximity was set to $1\mu\mathrm{m}$ and the number of cells across a gap was set to 5. These final two settings were the most important in determining the size of the fine portion of the mesh, which is where the velocity profile would be found. The rest of the settings (found in Quality, Inflation, and Advanced) were left at their default settings. The mesh can be seen below in Figure 2.10.

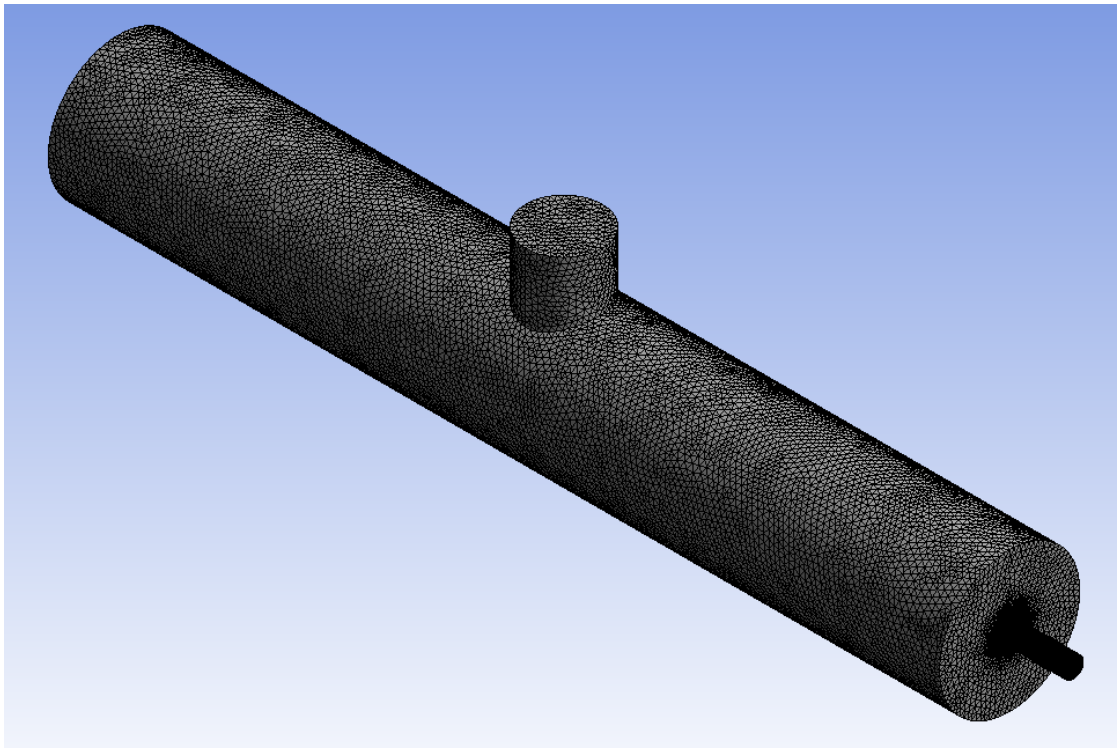

Figure 2.10: Meshed geometry for the CFX Simulations.

The setup for the simulation was performed in ANSYS CFX Pre, as shown in Figure . The default domain was set as water at 25°C with a reference pressure of 800 psi. It was analyzed as a continuous fluid and buoyant forces were neglected. Additionally, the domain was set to be stationary with no mesh deformation. This was because the simulation was run as at steady-state due to difficulties tracking colliding geometries for this case. The justification for running the simulation at steady-state can be found in Section 3.1. The CFX model used a Shear Stress Transport turbulence model, and turbulence intensity was assumed to be 10% at the inlet and outlet of the Pipe. Though they are referred to as the inlet and outlet of the Pipe for simplicity's sake, it is important to note that the inlet and outlet were both set as openings instead of inlets and outlets. This was because the pressure was prescribed and the flow was to be determined by the simulations. The inlet had a relative pressure set to 0 (meaning it was equal to the relative pressure), while the outlet had a relative pressure of -800psi, or atmospheric pressure. The walls of the Plug and Pipe

were modeled as rough walls with a roughness height of $150\mu\mathrm{m}$, a conservative roughness height for stainless and carbon steel.

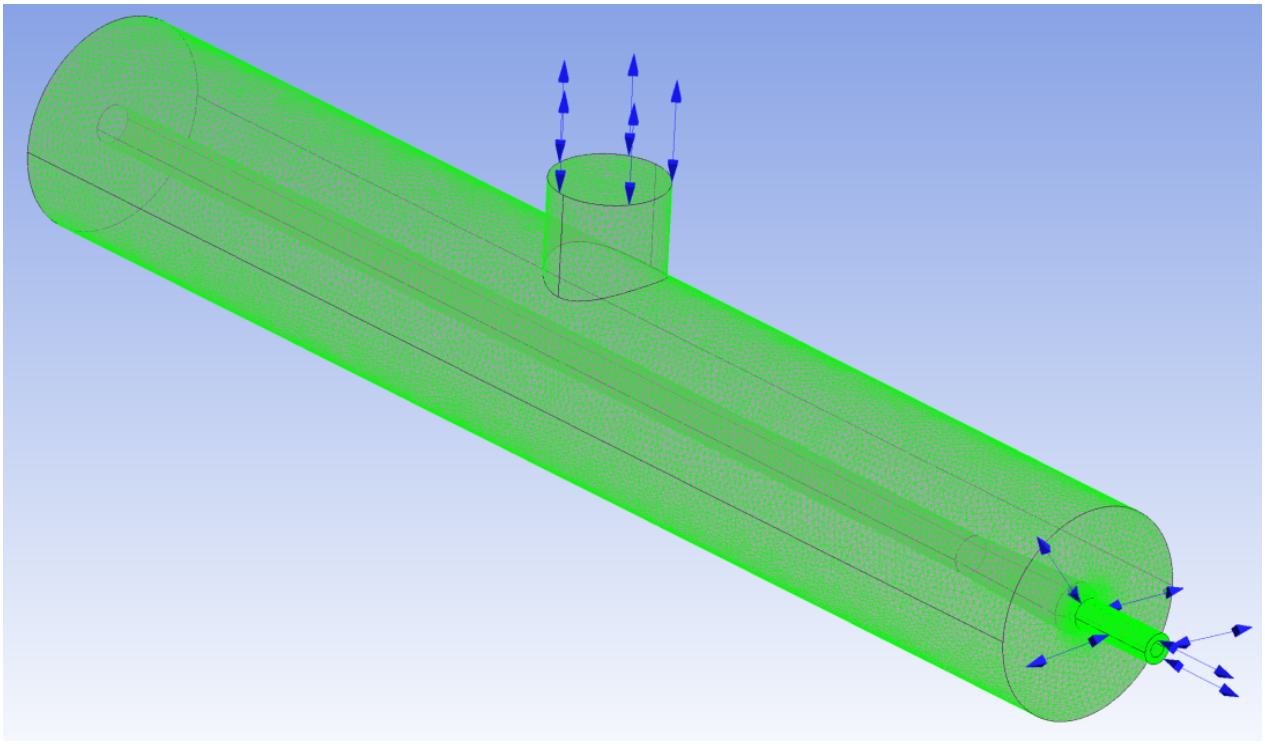

Figure 2.11: The prepped mesh for the CFX simulations with inlet and outlet set as openings.

The stop conditions set for the simulations were 300 iterations, or a convergence of all the residuals to below 10^{-5}. The max iterations were later set to 600 as explained in Section 3.1.1. A brief explanation of CFD residuals follows.

Residuals serve as a measure of the imbalance of the control volume problem which is solved at each finite element. The higher the residuals, the more imbalance, which means that there is a higher level of inaccuracy in the model. CFX reports normalized residuals, which are normalized as shown below [20]:

$$\tilde{r_\phi} = \frac{r_\phi}{a_p \Delta_\phi} \tag{2.1}$$

Where ϕ is the solution variable for which the residual is being calculated, $\tilde{r_\phi}$ is the normalized residual, r_ϕ is the raw residual, a_p is a stand-in for the control volume coefficient (determined by CFX), and Δ_ϕ is a stand-in for the range of the variable in the domain being analyzed. Additionally, the residuals which will be discussed in this thesis are the RMS (Root Mean Square) residuals, as they are more representative of the simulation as a whole.

In general, there is a hierarchy of desirability for residual values in a CFD simulation. Based on ANSYS standards, this hierarchy can be summarized as follows [20]:

- RMS residuals above 10^{-4} are sufficient for a qualitative understanding of a given flow field
- RMS residuals equal to 10^{-4} show a somewhat loose convergence, but can be sufficient for many engineering problems
- RMS residuals equal to 10^{-5} show a good convergence for the problem, which is sufficient for most engineering applications
- RMS equal to 10^{-6} shows a very tight convergence. While this is occasionally required for highly specific problems, it is often impossible to reach this level of convergence

After each CFX simulation, ANSYS CFX Post was used to find the velocity distribution along the orifice. This was done by using the probe tool to sample the water velocity at designated points along the radial direction of the orifice. It was assumed that the flow was axi-symmetric by the time it reached the orifice. The justification for this assumption can be found in Section 3.1. Once the velocity distribution was obtained, MATLAB's $cftool$ program was used to curve fit a fourth order polynomial to the data. This polynomial was then plugged in to the Conservation of Linear Momentum Equation shown below:

$$\frac{\partial}{\partial t}\iiint_V \rho\vec{v}dV + \iint_A \rho(\vec{v}\cdot\hat{n})\vec{v}dA = \iint_A -p\hat{n}dA + \iiint_V \rho\vec{g}dV + F \tag{2.2}$$

It is important to note that many curve fitting software tools, MATLAB's $cftool$ included, offer a centering and scaling feature which allows the polynomial coefficients to maintain much more manageable magnitudes. Using this feature, however, makes the equation lose its physical significance, and it becomes a purely mathematical representation. In order to use the velocity distribution to calculate F_{jet} and the flow requirements of the shaker, the curve fit was not centered and scaled.

As stated above, the simulations were steady-state, and the pressure outside of the orifice was atmospheric. The calculation of the Reynold's number can be found below. For flow through a small orifice, 10^5 is high enough to consider the flow to be inviscid [21]. Therefore Equation (2.2) simplifies to Equation (2.4).

$$\begin{aligned} Re &= \frac{\rho u L_c}{\mu} \\ &= \frac{(1000[\frac{kg}{m^3}])(60.1[\mathrm{m/s}])(2.03[\mathrm{mm}])}{8.90 * 10^{-4}[\mathrm{Pas}]} \end{aligned} \tag{2.3}$$

$$F_{jet} = \iint_A \rho(\vec{v} \cdot \hat{n})\vec{v}\, dA \tag{2.4}$$

Where ρ is the density of water, $\vec{v}$ varies with radial position and is pulled from the velocity distribution, $\hat{n}$ is the unit normal vector pointing outwards from the orifice, and A is the cross-sectional area of the orifice through which fluid flows. F_{jet} is the force of the water jet, a value which is used extensively throughout the rest of this paper.

Finally, the required flow rate of the shaker was calculated based on the Law of Conservation of Mass.

$$\frac{\partial}{\partial t} \iiint_V \rho dV = \iint_A \rho \vec{v} \cdot \hat{n} dA \tag{2.5}$$

For constant density, this can be stated as the much more straightforward (and desirable) Equation (2.6).

$$\dot{q} = \iint_A \vec{v} \cdot \hat{n} dA \tag{2.6}$$

This is integrated similarly to Equation (2.4), with the velocity varying with position as the velocity distribution. Because of the length of the pipe, as well as the interrupted flow provided by the Plug, it was assumed that the velocity profile, by the time the fluid got to the orifice, was axisymmetric, meaning that in the plane of the orifice the flow only varied in the radial direction. This allowed for a simple 1D approach to find thrust.

Additionally, there was initial concern that the pressure within the shaker would prevent the Plug for being pushed from one FOFC position to the other. The pressure at the orifice is expected to be significantly lower than the 800 psi within the Pipe. The force due to pressure at the orifice can be found by the following equation:

$$\begin{aligned} F_{pressure} &= \iint_A P \cdot dA \\ &= \int_{r1}^{r2} \pi P r dr \end{aligned} \tag{2.7}$$

The force due to pressure on the Plug was found to be negligible, as can be seen in Section 3.1.1.

2.2.2 System Dynamics

For the system dynamics, the general equation of motion is given as:

$$m\ddot{x} + c\dot{x} + kx = F \tag{2.8}$$

This problem is made simple by the fact that it is a single degree of freedom problem (single axis vibration). The calculation is, however, complicated by the fact that the k, c, and F are piecewise functions of position. A collection of springs and dashpots were used to describe the conditions faced by the shaking unit within the housing of the desalination unit. This can be seen below in Figure 2.12.

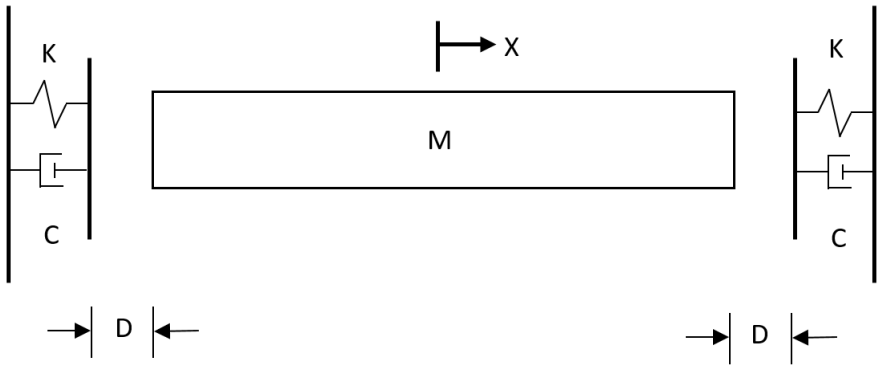

Figure 2.12: Simplified visualization of the wall reactions on the shaker as it vibrates.

Where D is the distance between the shaker (at its neutral position) and the wall, K is the stiffness of the wall, C is the inherent damping of the wall, m is the mass of the membrane assembly, and x is the x coordinate of the unit with zero being set at the neutral position. Since the parameters were to be based on that of a steel wall, a damping ratio (ζ) of 0.005 and an initial stiffness (k) of $10^{10}\mathrm{N/m}$ were used. The distance D was set to $1\ \mathrm{mm}$.

In order to model these nonlinear dynamics, the function osc_motion was created. This is where the values of D, K, C, and M were input. The piecewise force function for the water jet and wall can be seen below in Equations (2.9) and (2.10).

$$F_{wall} = \begin{cases} -k(x+D) - c\dot{x}, & x < -D \\ -k(x-D) - c\dot{x}, & x > D \\ 0, & else \end{cases} \tag{2.9}$$

$$F_{propulsion} = \begin{cases} F_{jet}, & x < -D + D(0.5) \text{ and } \dot{x} \leq 0 \\ -F_{jet}, & x > D - D(0.5) \text{ and } \dot{x} \geq 0 \\ 0, & else \end{cases} \tag{2.10}$$

Where F_{wall} is the force exerted on the shaker by the wall, $F_{propulsion}$ is the force that is propelling the shaker, and F_{jet} is defined in Equation (2.4). In addition to these forces, there was also an assumed frictional force of 5% of the weight, bringing the total equation of forces to:

$$F_{wall} + F_{propulsion} - F_{friction} = m\ddot{x} \tag{2.11}$$

This final expression was put into osc_motion to find the acceleration of the system. The equation was then solved using MATLAB's $ode45$ to find the graph of position vs time.

It is important to note that, during the process of running the simulations, the values of k and $F_{friction}$ were changed to $10^8 \mathrm{N/m}$ and 4.25% of the weight, respectively. These changes are further explained in Section 3.1.2.

In order to properly determine the parameters for the experiment, it was necessary that a series of simulations be performed. F_{jet}, defined in Equation (2.4), was obtained by running ANSYS CFX simulations (discussed above in section 2.2.1). D, k, and c are predetermined by the setup of

the problem. D is based on the amplitude of vibration required to have the desired reduction on membrane fouling. k and c are determined based on material properties and assumed geometry for the walls inside the housing of the desalination unit.

After each time the problem was solved, the position vs time data was put into a FFT to determine if it matched the proper dynamic characteristics. If it did not, adjustments were made to the SolidWorks model to change the CFX model's output of F_{jet} so that it would provide the proper characteristics.

There was consideration for the inclusion of the acoustic and collision effects, but after running the dynamic simulation, it was found that the order of magnitude of these effects was small enough that they could be ignored. Though they were negligible for this particular case, the order of magnitude of the collision and acoustic effects of the shaker are still calculated for in osc_motion, so that if they become non-trivial, a warning is sent to the user.

Additionally, there was concern initially that the energy of the Plug collision would be enough to affect the dynamics of the shaker. However, the manufactured Plug, as seen in Figure 2.19 was found to have 0.06 kg of mass. Compared to the connected mass of the shaker and membrane unit of roughly 30 kg, this mass is only 0.2% of the total mass of the shaker. This means the inertial effects of Plug collision can be ignored for the model.

2.2.3 Scaling Up

In an effort to provide a robust aid to future research in the area, a series of up-scaling simulations were also performed. These were aimed at determining the amount of mass that could be shaken for each prescribed case. Since this particular project was based on a test size membrane, it was important to show that this shaking system would be capable of operating with larger membranes.

A series of CFX simulations were run to determine the force output and required flow for various values of length, Pipe diameter, and orifice diameter. The values tested are listed below:

- Pipe Length: 7 in, 4 in

- Pipe Diameter: 0.5 in, 0.75 in, 1.1 in
- Orifice Diameter: 0.16 in, 0.2 in 0.25 in, 0.3 in, 0.35 in

The simulations were run using the OFAT (One Factor At a Time) method to determine the effects of each factor on the value of F_{jet}. Based on the findings stated in 3.1.3, only the orifice diameter was varied for the up-scaling model.

The force values for the various orifice diameters were then put into a MATLAB script called $Orifice\_Optimization$ (see Appendix B). $Orifice\_Optimization$ calculated the amount of mass that could be shaken at the proper frequency for a range of wall stiffness values and a given F_{jet} value based on orifice size. The stiffness was varied from $10^5 \mathrm{N/m}$ to $10^8 \mathrm{N/m}$. This was then run for each force value for a given Pipe size. This was accomplished by iteratively solving for the position vs time information based on the current iteration's mass, stiffness, and F_{jet} values. This was then put into a FFT to determine the shaking frequency for the current iteration. $Orifice\_Optimization$ also adjusted the $F_{friction}$ to be 4.25% of the weight of the current iteration, based on findings in 3.1.2. If the shaking frequency was within a range of 1.5Hz of the target 20 Hz, then the simulation advanced to the next stiffness value. If not, then the mass was adjusted accordingly (increased if the frequency was too high or decreased if the frequency was too low), and then the iteration was run again. Initially, a static mass adjustment was used, but, as the simulation approached higher stiffness valued, it was found that the simulation was unable to converge. This was because, at high stiffness values, small changes in mass can have large effects on the shaking frequency. In order to account for this, an adaptive mass adjustment was used based on the current iteration's stiffness value.

2.3 Experimentation

2.3.1 Hardware

The experiment rig was built based on the specifications of the SolidWorks model. The engineering drawings for each part can be seen in Appendix A. Each component of the rig was designed to be assembled with bolts so as to ensure ease of adjustment. Since this experiment was purely to

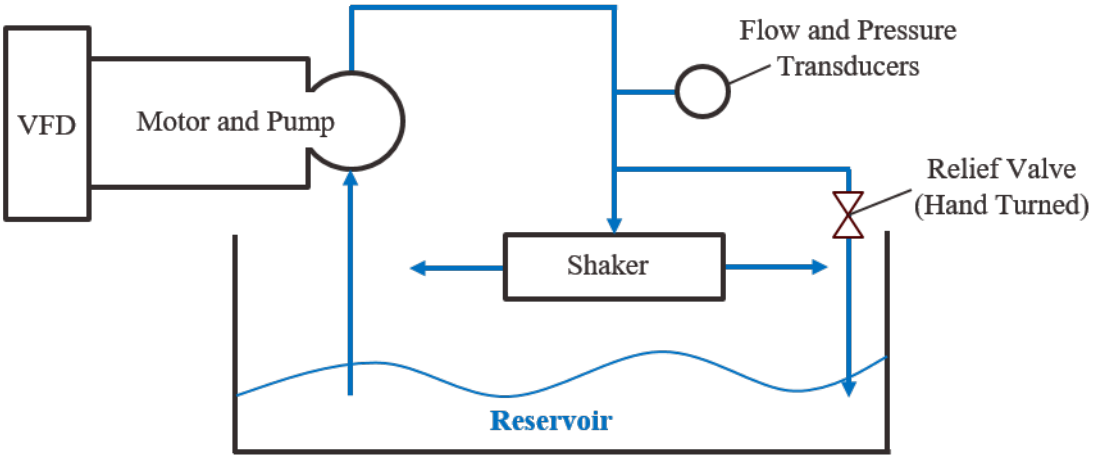

Figure 2.13: Simplified PFD of the experiment rig.

prove the concept of a water jet driven shaking device, the shaker was not attached to an existing CRO unit. Instead, a gear pump was used to get the water up to 800 psi and put straight into the shaker. The required flow was determined by simulation and can be found in Section 3.1. A basic outline of the experiment rig can be seen in Figure 2.13.

There was one change that had to be made in order to make the Plug more easily manufacturable. In order to greatly decrease cost, the Plug was split into three pieces. The dumbbell-shaped portion remained one piece, but instead of the two rods sticking out on either end, they were removed and a threaded hole was bored into the Plug. The two small rods that stick out on either side were made separately and threaded so that they could screw into the Plug. This was the only change to the design that manufacturing brought about. The engineering drawings in Appendix A show the final Plug design. The manufactured Plug assembly can be seen in Figure 2.14.

Table 2.2: Motor specifications

Specification	Value
HP	3
Volts	230
Amps	9.0
rpm	1760
HZ	60
Phase	3

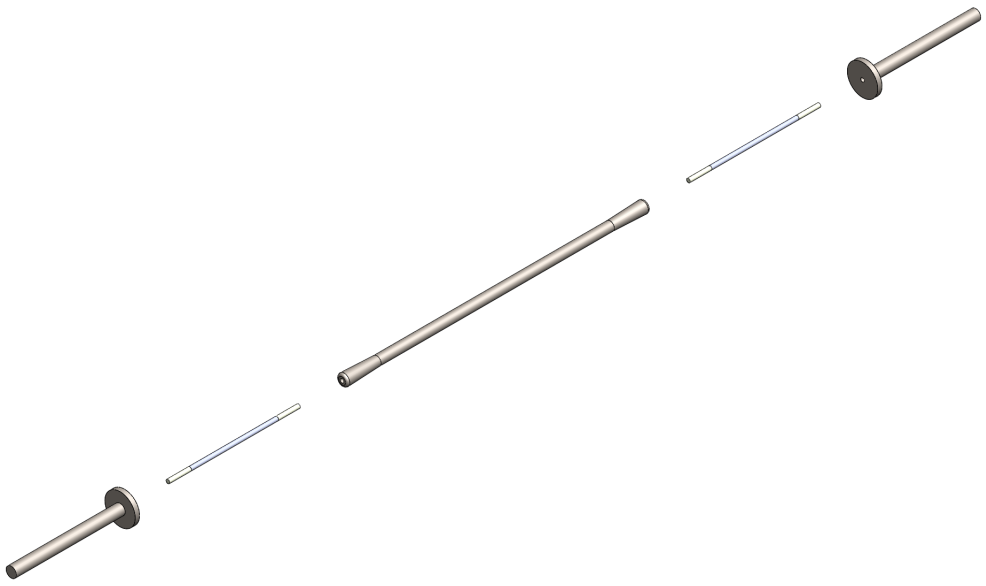

Figure 2.14: Full Plug assembly after being adjusted for manufacturing purposes

The pump and motor purchased were the Bosch Rexroth MPGB003HTYZ4DEOFS1AZPF12014K1NN, which is a coupled motor and gear pump group with an internal coupling. The motor specifications and pump performance curve can be seen in Table 2.2 and Figure 2.15.

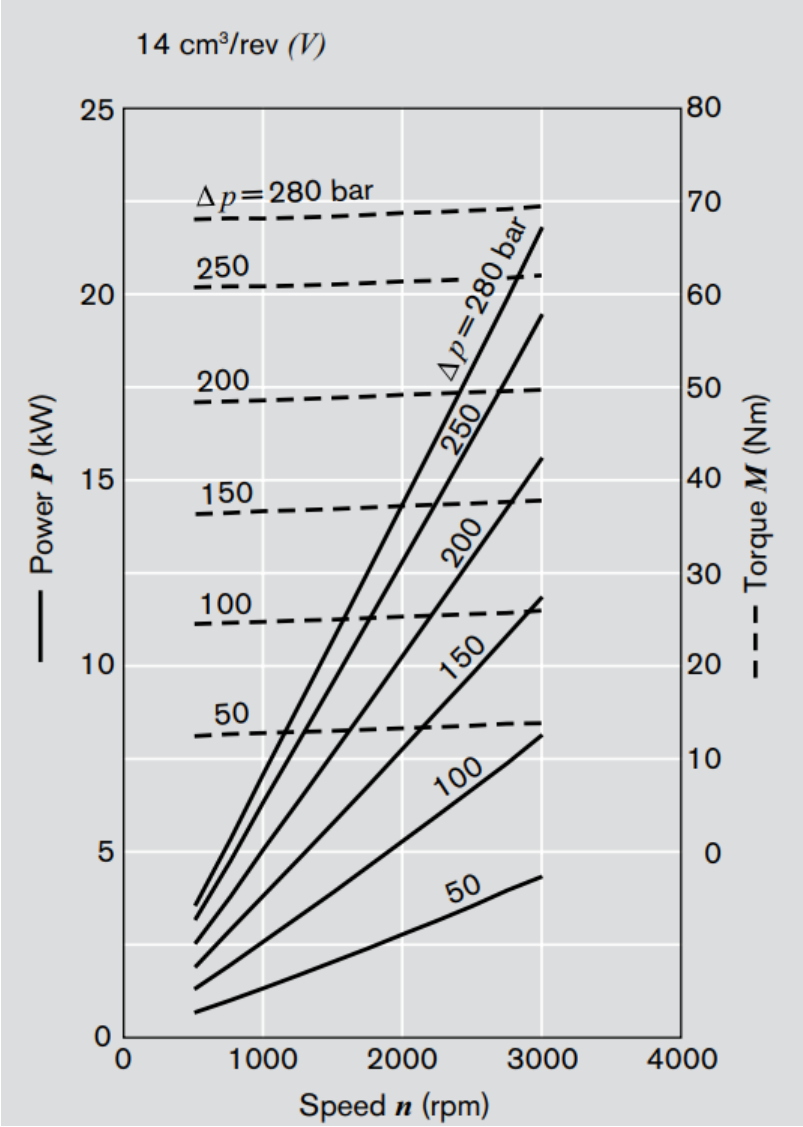

Figure 2.15: Performance curve for the gear pump. Reprinted from "External Gear Pumps, Series F" [22]

In order to have full control over the flow of the pump, the motor was connected to a VFD (Variable Frequency Drive). The VFD was a 5 HP DURAPULSE from Automation Direct. Pictures of the pump and motor, as well as the VFD can be seen below, along with the VFD specifications for the run. The input frequency varied based on each experiment being run. In order to avoid damage to the motor, the input frequency was maintained between 55 Hz and 65 Hz. The assembled pump and motor, as well as the VFD can be seen in Figures 2.16 and 2.17, while the VFD specifications

Figure 2.16: Bosch Rexroth gear pump and induction motor used for experiments.

can be found in Table 2.3.

An auto-tune for the motor was performed, which determined the motor resistance was 1100 Ω, and the motor no load amperage was 2.7 A. It is important to make sure the motor and pump are not hooked up to the system when performing an auto-tune.

The flow transducer was an in-line Headland variable area flow meter, capable of measuring up to 10 $\mathrm{gal/min}$ with up to 1000 psi of pressure. The pressure transducers were dual-scale, steel cased pressure gauges with capacity of measuring up to 1000 psi.

Because there were such high pressures involved in this experiment, safety was a major con-

Figure 2.17: Automation Direct VFD used for experiments.

Table 2.3: VFD specifications

Specification	Value
Motor Voltage	230 V
Motor Amperage	9 A
Motor Frequency	60 Hz
Motor Base RPM	1760 rpm
Motor Max RPM	1900 rpm
Motor Auto-Tune	1
Motor Resistance	(determined by auto-tune)
Motor No Load Amperage	(determined by auto-tune)

Figure 2.18: The manufactured and assembled shaker.

Figure 2.19: The manufactured and assembled Plug, which sits inside the shaker.

cern. In order to mitigate any potentially damaging incidents, all piping used was schedule 160 steel pipe with class 3000 fittings. This ensured that the rig was safe for any over-pressure scenario.

Pictures of the manufactured shaker can be seen below. The Pipe needed to be capable of holding high pressures without ever failing, so significantly strong metal was needed. Because the Pipe had no sliding or moving parts (though the Pipe itself moved as a whole), there was no need to consider the effects of oxidation. In order to cut down on costs, the Pipe was made of A36 steel. This also allowed for much easier machining than if stainless steel was required. The small dimensions of the Plug, however, did require a stronger metal in order to be manufactured reliably. Thus, the Plug was made of 304 stainless steel. The end caps also needed to be sufficiently strong in order to hold the pressure while only being held by a bolted circle. Since these parts also did not move (other than as a whole) A36 was used for these as well. The shaker base and end plates were all made from 6061 aluminum, as they had lower strength requirements due to the fact that they were not required to hold pressure. The manufactured parts can be seen in Figures 2.18-2.23.

The rest of the parts used in the rig setup were COTS. Their details can be seen in the BOM

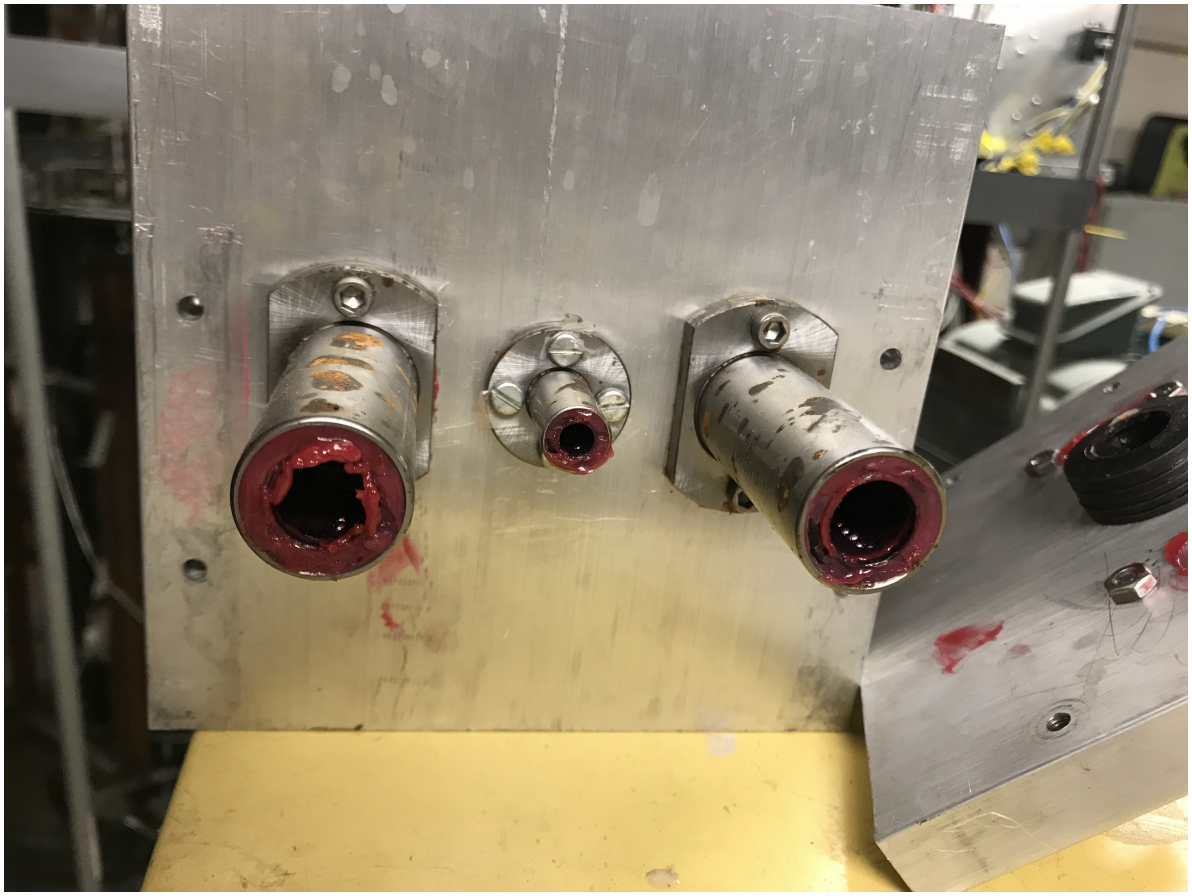

Figure 2.20: The manufactured end plate with purchased linear bearings attached

Figure 2.21: The manufactured and assembled shaker base sitting over the reservoir.

Figure 2.22: The assembled shaker and base sitting on the rig, with shielding curtain pulled back.

Figure 2.23: The fully assembled test rig, with shielding curtain to protect the motor from the water sprayed by the shaker

(bill of materials) in Table 2.1.

2.3.2 Experiment Setup

First, a test was performed to ensure the water jet was providing sufficient force to move the mass of the shaker. The shaker was suspended by the hose and the water pressurized and sent to the shaker. The angle the shaker was pushed to by the jet was then measured to determine the force. This was not meant to be a particularly rigorous test, but more of a preliminary proof that the flow was providing sufficient force, and there were no blockages or major leaks in the system. The force of the water jet can be found as follows:

$$F_{jet} = F_{weight} * sin(\theta) \tag{2.12}$$

Where θ is the angle to which the jet pushes the shaker.

Next, the shaker was detached from the hose and assembled with the end plates and linear bearings, but not the shaker base. This setup is shown in Figure 2.24. This was done to ensure that there was no misalignment of the shafts and bearings.

Next, the shaker was attached to the hose and slid into the plates. The plates were then attached to the base as shown in Figures 2.25 and 2.26. Before turning the VFD on, the relief valve was set to fully open. The VFD was then turned on and set to 55 Hz. Then, as the water began to flow, the relief valve was slowly tightened until the pressure of the system was around 500 psi. Next, the frequency on the VFD was increased until the flow meter showed the desired amount. While increasing the frequency of the VFD, it is important to monitor the pressure in the system. If the flow through the orifice is insufficient, it can lead to an over-pressure scenario. In the event of an over-pressure situation, it is important to quickly press the STOP button on the VFD and open the relief valve more before re-starting the test. Once the proper frequency and relief valve settings were found, the shaker was pushed to be fully-open-fully-closed (FOFC), or the position where one orifice is completely sealed and the other is completely open. Then the shaker was to be observed to ensure it was shaking properly.

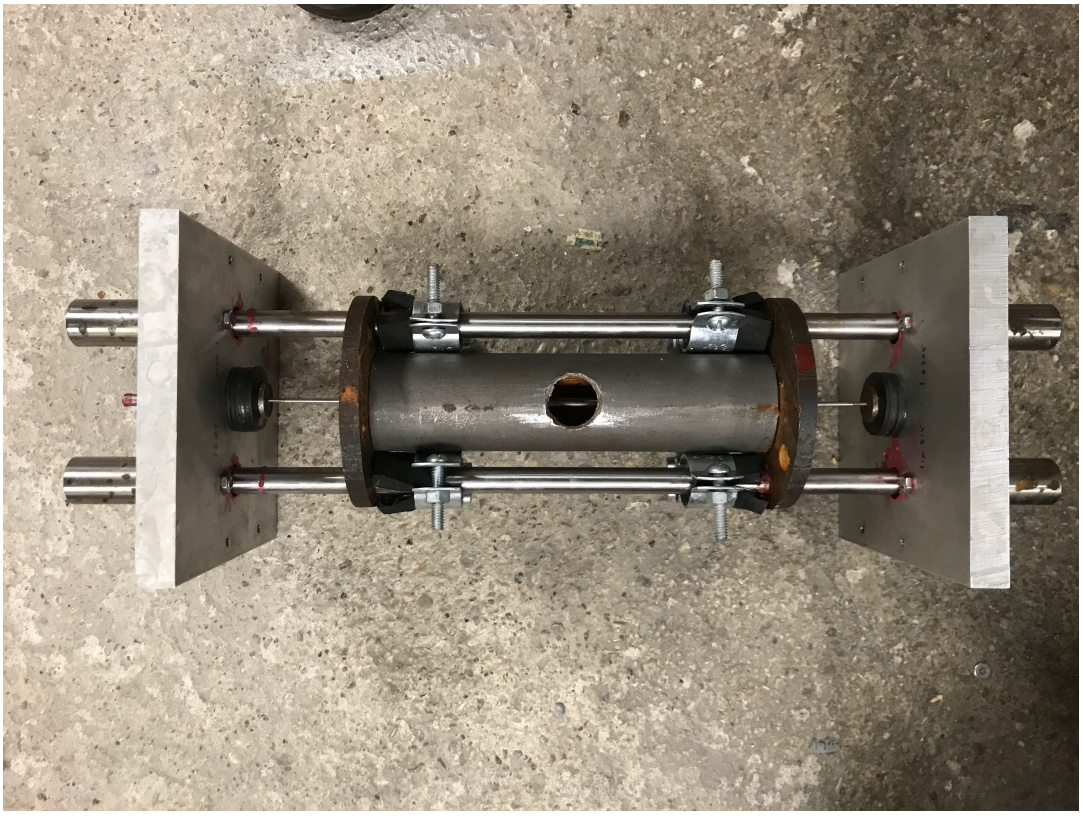

Figure 2.24: The shaker being tested for shaft misalignment

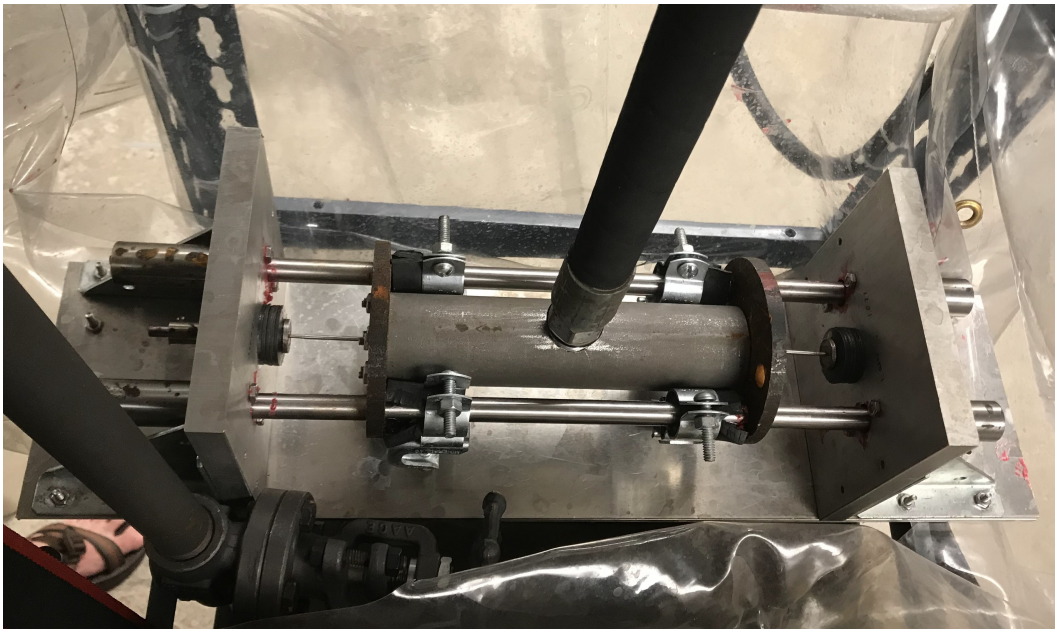

Figure 2.25: Overhead view of the shaker on the rig

Figure 2.26: Picture of the overall rig between runs

If the shaker had been able to shake, a DAQ (Data Acquisition) system would have been outfitted to the rig, with proximity sensors attached to the end plates. Further explanation as to the reason this was not done can be found in Section 3.2.

3. RESULTS AND DISCUSSION

3.1 Simulations

This section details the results of the simulations which determined the parameters of the experiments. As may be expected, the simulations detailed in Section 2.2 were iterated upon many times. After each series of simulations, the output of the position vs time data (see Figure 3.4) was analyzed to check for the proper amplitude and frequency and to ensure that the vibration was stable. A FFT of the shaker motion would then be performed to find the shaking frequency to determine if it was in the acceptable tolerance of 1.5 Hz. If adjustments needed to be made, the geometry was slightly changed, and then the series of simulations were run again until the proper dynamic characteristics were achieved. The simulation results for the CFX simulations, the MATLAB simulations, and the up-scaling simulations are found in Subsections 3.1.1, 3.1.2, and 3.1.3, respectively.

3.1.1 Fluid Mechanics

The final CFX output can be seen below in Figure 3.1. As expected, the flow is mostly zero throughout the body of the Pipe. It is only near the orifice that the velocity increases due to the large pressure difference between the water in the Pipe and the atmosphere. In Figure 3.1, the Plug can be seen as a blue body in the center of the Pipe, which is the wire frame surrounding the flow. Additionally, it is important to note the residuals graph in Figure 3.2. It took nearly 400 iterations before the residuals were able to fall below 10^{-4}, and they were not able to reach 10^{-5}. It was decided, however, that this level of convergence was sufficient to determine the characteristics of the experiment rig, as adjustments could be made with the VFD or by adjusting the hand-turned relief valve.

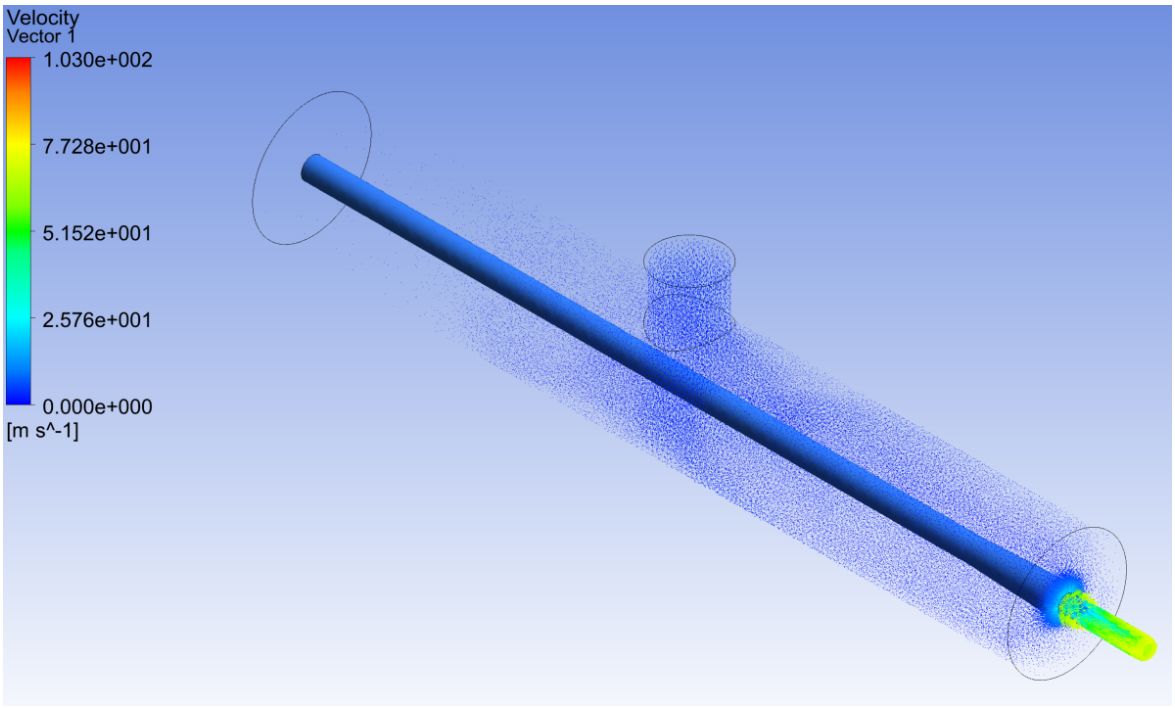

Figure 3.1: CFX results for the case of a 1.1in ID Pipe and a 0.16 in^2 orifice which has 0.085 in^2 blocked by the Plug.

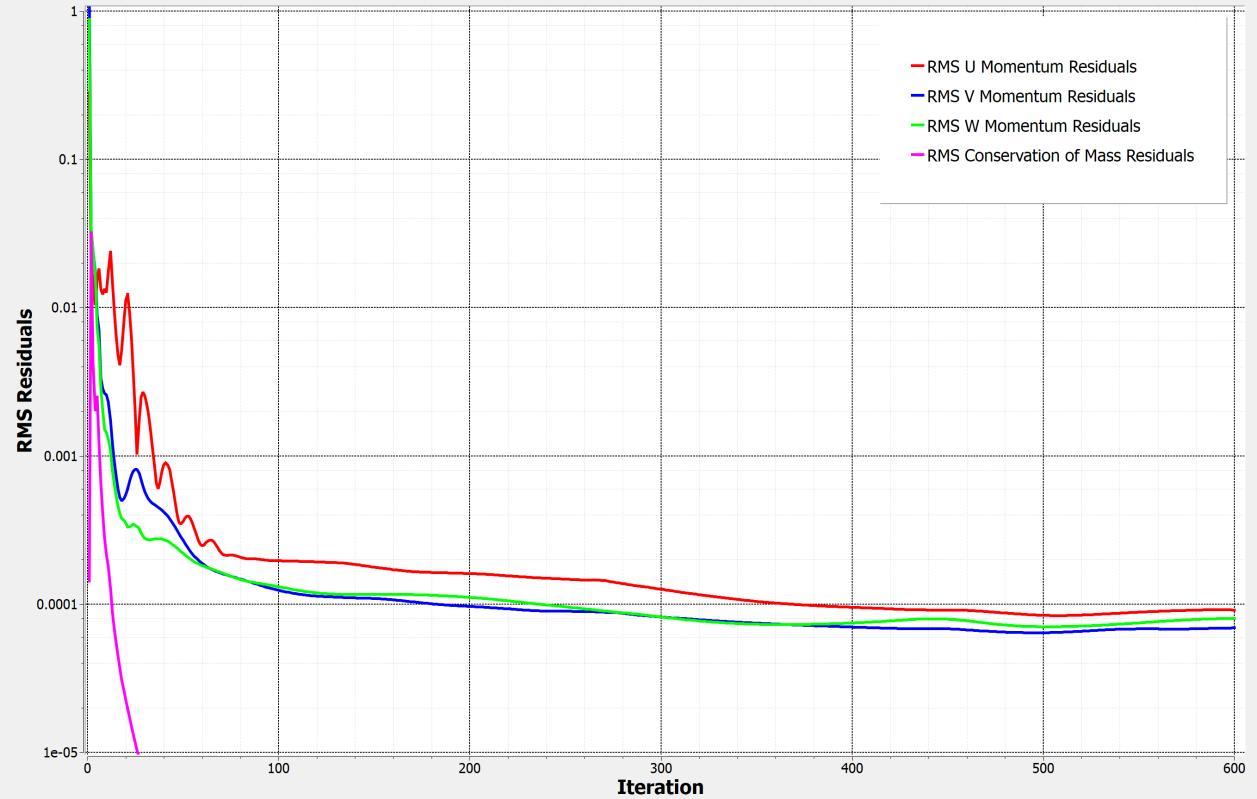

Figure 3.2: CFX RMS residuals for the case of a 1.1in ID Pipe and a 0.16 in orifice which has 0.085 in blocked by the Plug.

This CFD model was then used to determine the velocity profile of the flow through the orifice. The discrete velocities can be seen in Table 3.1. Using $cftool$ in MATLAB, the velocity profile was found and can be seen in Equation 3.1.

$$\vec{v}(r) = (3.856 * 10^{13})r^4 - (3.492 * 10^{11})r^3 + (9.511 * 10^8)r^2 - (1.012 * 10^6)r + 424.2 \quad (3.1)$$

This curve fit, which can be seen in Figure 3.3, provides a R^2 value of 0.9987, which describes the data excellently. The coefficients for the curve fit are quite large and vary significantly in order of magnitude. This is because the velocity has large changes over such a small gap. The discrete velocities shown in Table 3.1 also prove that the assumed average velocity in Equation 2.3 was a

Table 3.1: Discrete fluid velocities along the radial direction for the 7in long, 1.1in diameter Pipe with a 0.16in orifice

Position along the orifice radius [mm]	**Velocity** [m/s]
1.09	53.3756
1.20	56.2295
1.30	59.1962
1.40	61.5445
1.50	62.8178
1.60	61.626
1.70	60.2974
1.80	52.2877
1.90	42.1128
2.00	27.6163
2.03	22.9775

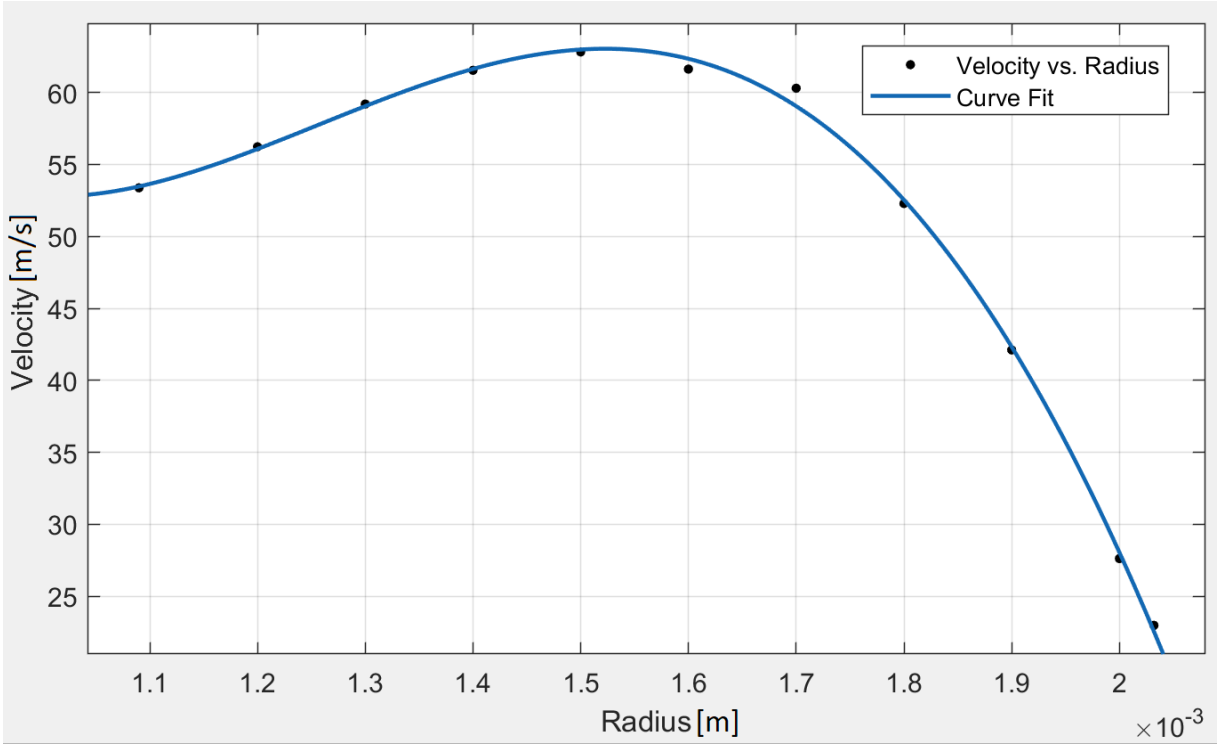

Figure 3.3: The discrete values and curve fit for the 7in long, 1.1in diameter Pipe with a 0.16in orifice

good basis off of which to make the inviscid assumption.

Plugging Equation (3.1) into (2.4) gives:

$$F_{jet} = 27.13\text{N} \tag{3.2}$$

A series of simulations was performed to test the variation of force output as a function of distance from plug to orifice. These results can be seen in Table 3.2. At first glance, it may seem that the force output increases in a somewhat linear fashion as the Plug moves away from the orifice, however it is important to remember that, when the Plug is not fully closing one of the orifices, there is flow coming out of both sides. During this time, the corresponding force output should be subtracted from whichever output is being observed. For example, when the Plug is 0.5 mm away from the orifice there is a force of 11.8 N coming from that orifice, as well as a force of 18.2 N in the opposite direction from the other orifice. Because the force is sufficiently small and the time that the shaker stays in this state is sufficiently short, these nonzero reaction forces were considered negligible for the sake of modeling the dynamics. Therefore the orifice was modeled as being fully open or fully closed, with no intermediate conditions considered in the model. This allowed for a much more simplified dynamic model.

Table 3.2: Force output at varying distances between the Plug and orifice

Distance (mm)	**Force Per Shaker** (N)	**Force Per Shaker** (lbf)
0	0	0
0.25	9.19	2.07
0.5 (left side)	18.78	4.22
0.5 (right side)	18.29	4.11
0.75	24.02	5.40
1.0	27.13	6.10

Additionally, an analysis of the flow requirement was performed. As stated in Section 2.1, the flow must remain small in order for the method to be viable. Equation (2.6) was integrated numerically to give the flow requirement. For the final case, the flow required was found to be 7.78 gpm, which was sufficiently below the flow through the full system, which is expected to be around 32 gpm [8].

As stated in Section 2.2.1, there was some concern early on that the pressure in the Pipe would prevent the Plug from being able to move from the FOFC position. After further analysis, however, this proved to be baseless. This is because the pressure within the shaker, though 800 psi throughout most of the Pipe, is much much lower at the open orifice due to the flow. The pressure distribution at the orifice was found the same way the as the velocity distribution, meaning the pressure at discrete points was found and then curve fit with MATLAB's $cftool$. The pressure distrubution can be seen below in Equation (3.3), where the units have all been converted to SI.

$$P(r) = (-1.954*10^{19})r^4 - (1.134*10^{17})r^3 - (2.409*10^14)r^2 + (2.239*10^11)r - 7.335*10^7 \quad (3.3)$$

This pressure distribution was then put into Equation (2.7), and the resulting force was found to be $F_{pressure,orifice} = -12.57\mathrm{N}$. The force due to the pressure for the rest of the pipe was solved similarly, but with a constant distribution of 800 psi. The force due to this pressure was found to be $F_{pressure,Pipe} = 16.22\mathrm{N}$. This means the net force required to move the pipe is $3.65\mathrm{N}$, which is far below the $27.13\mathrm{N}$ provided by F_{jet}. Thus, the Plug was proven to be easily moved even in the presence of high pressure.

3.1.2 System Dynamics

The results of MATLAB's ode45 solver solving the equations in Section 2.2.2 can be seen below in Figure 3.4. Duing the first second, the ramp-up of the motion can be seen, and the motion steadies out after two seconds. The red lines at the top and bottom of the graph represent the walls on either side of the shaker.

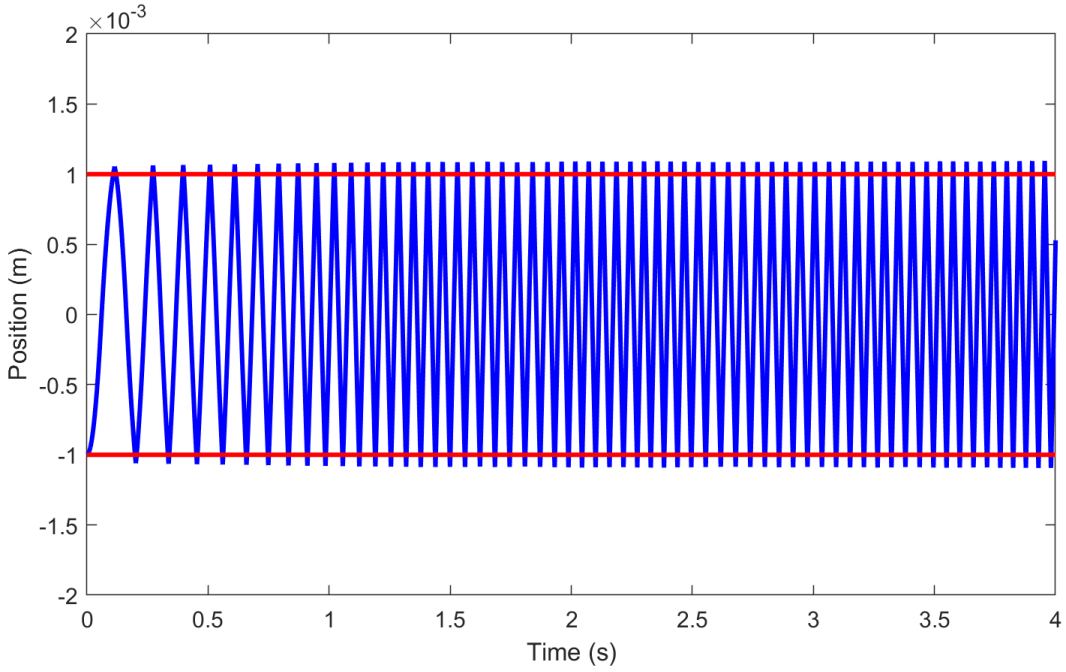

Figure 3.4: Position vs time for the motion of the shaker in its first four seconds of run time, based on a 1.1in ID Pipe and a 0.16in^2 orifice which has 0.085in^2 blocked by the Plug.

It can be seen in Figure 3.5 that more than one mode is being excited in this shaking. The nonlinearity of the motion likely contributes to this phenomenon. The two major peaks in the frequency spectrum graph are at 17 Hz and around 25 Hz. The motion itself actually averages out to be shaking at around 18.9 Hz, which is within the 1.5 Hz tolerance set at the beginning. Thus, these dynamic characteristics were acceptable.

It is important to note that, in order to achieve these dynamic characteristics, there were some slight changes required of the parameters. For example, it was found that the friction in the system had a maximum value, above which the system becomes overdamped. This maximum value was 4.5% of the weight of the membrane unit. The overdamped motion of the shaker can be seen in Figure 3.6. In order to avoid this, the friction force in the model was reduced to be 4.25% of the membrane unit's weight. Based on the 28 kg mass discussed in Section 2.2.2, the friction force was equal to 11.67 N for this particular case. Additionally, the k value of the walls was reduced to 10^8N/m, as the initial value of 10^{10}N/m was found to be both difficult to achieve in the context of

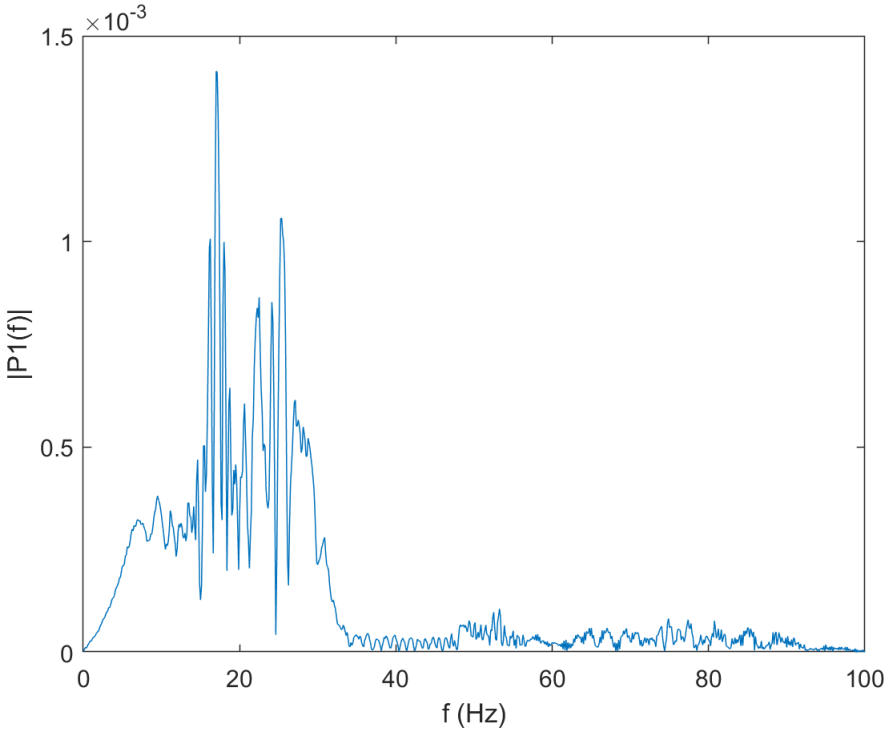

Figure 3.5: Frequency spectrum analysis of the motion of the shaker

full system implementation, as well as unnecessary for the required dynamics of the system.

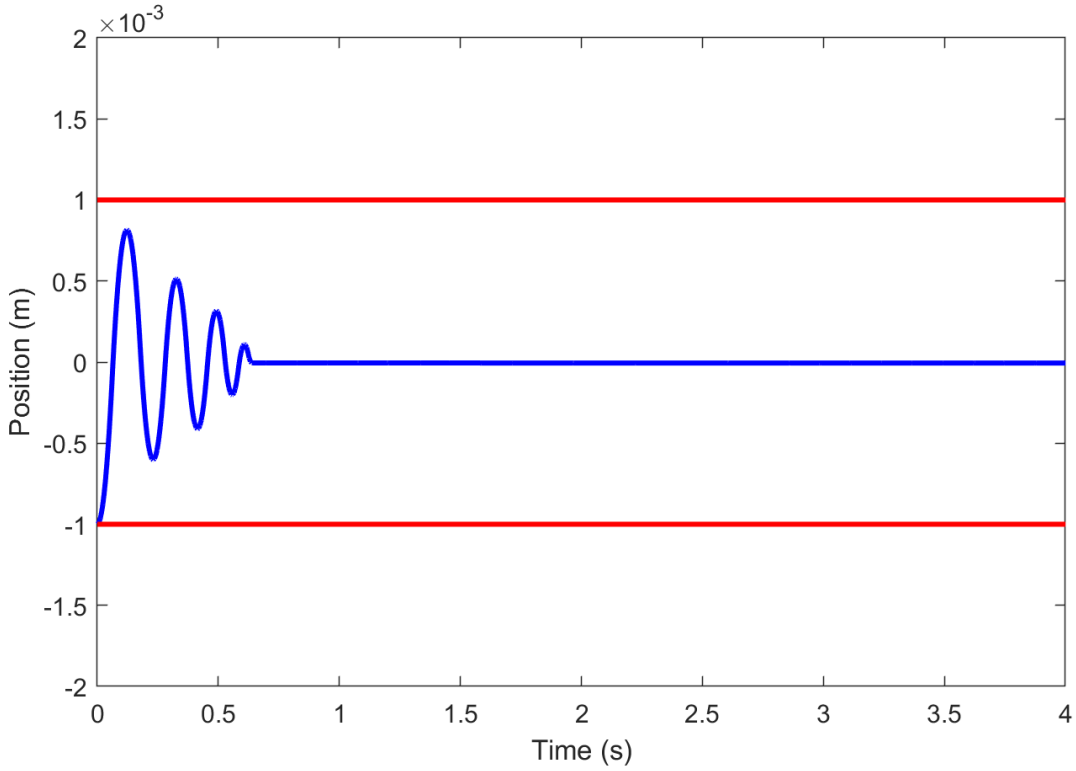

Figure 3.6: Position vs time for motion of the shaker with a friction force of 4.6% of the membrane unit's weight.

Another point to discuss is that these simulations showed that it is crucial for the shaker to start from one of the extreme positions, and not in the equilibrium position. This is because there is no force acting upon the shaker when it is at the zero position. F_{jet} and F_{wall} only act at or near the extremes of the shaker's motion. The only other force present is $F_{friction}$ which, of course, will not drive any motion. Therefore it was important to ensure the shaker was at one of its extreme positions when each experiment was performed.

3.1.3 Scaling Up

A comparison of the F_{jet} value for varying lengths and diameters can be seen in Table 3.3 and Figure 3.7.

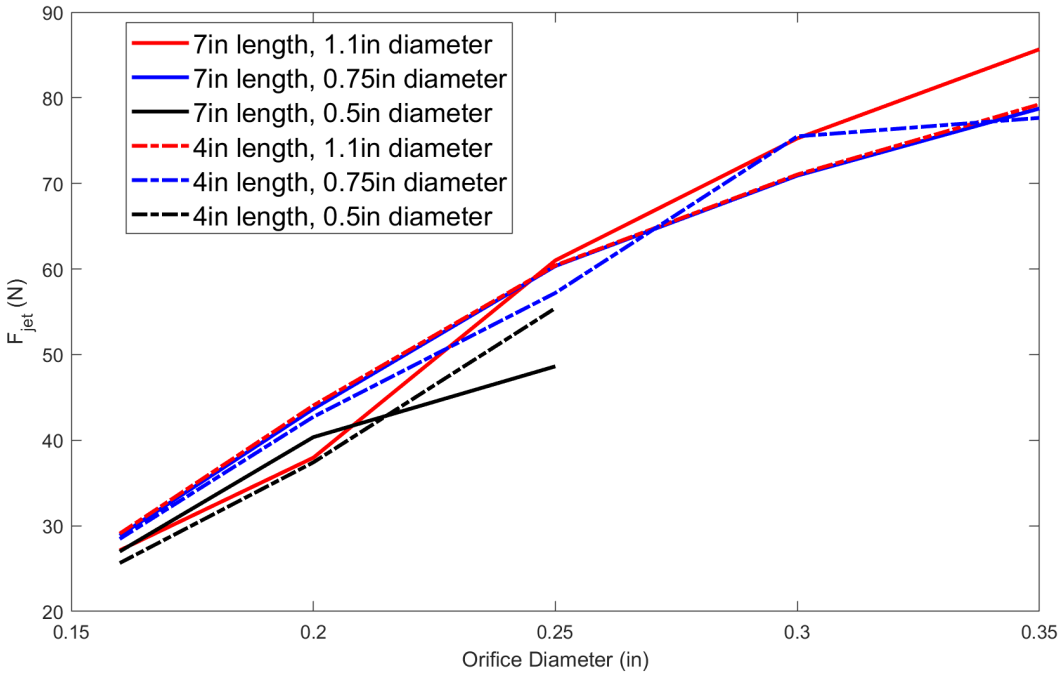

Figure 3.7: Graphical representation F_{jet} for varying pipe configurations

Table 3.3: Comparison of force per shaker for varying pipe sizes

Orifice Diameter (in)	**Force per shaker** (N)					
	7in Length			4in Length		
	1.1in	0.75in	0.5in	1.1in	0.75in	0.5in
0.16	27.13	28.86	27.00	29.09	28.46	25.65
0.2	37.95	43.65	40.36	44.06	42.73	37.41
0.25	61.01	60.35	48.63	60.42	57.21	55.43
0.3	75.26	70.91	N/A	71.04	75.50	N/A
0.35	85.67	78.75	N/A	79.24	77.65	N/A

It is important to note that the 0.5 in diameter pipe simulations were not run with an orifice diameter above 0.25 in. This is because the ratio of plug to pipe was too large and the simulation

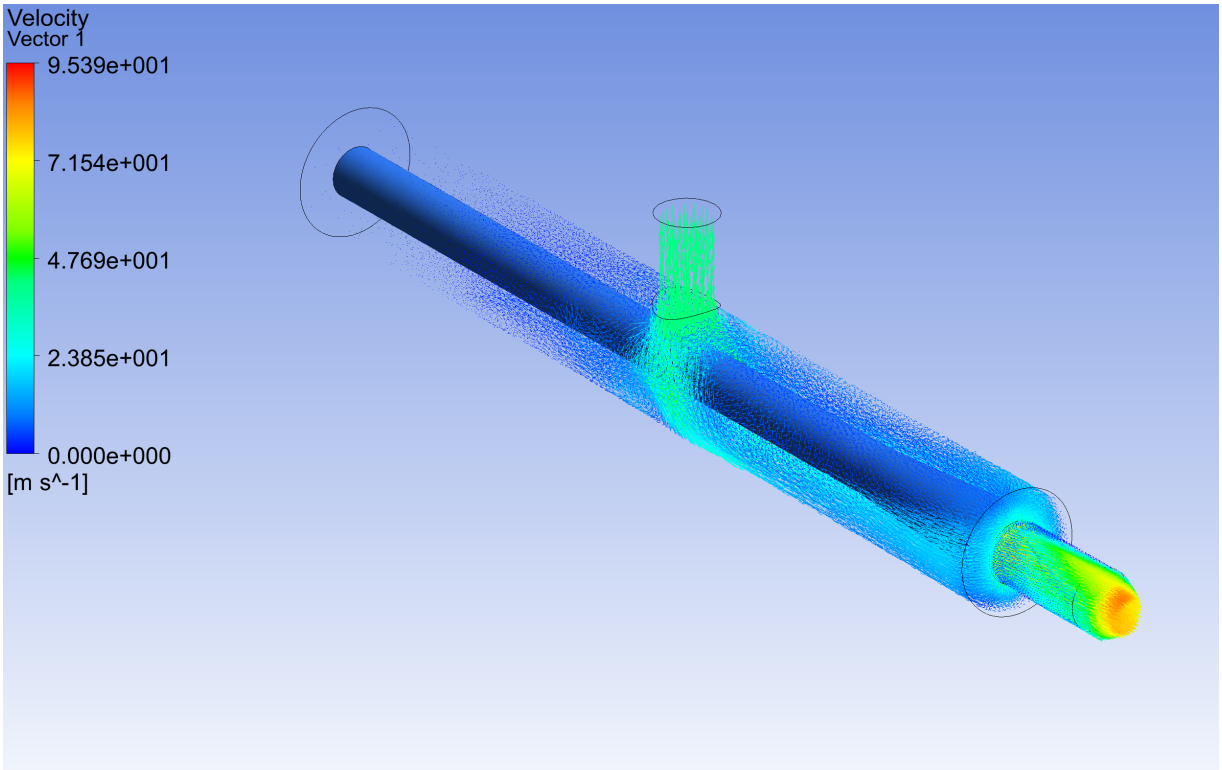

Figure 3.8: Flow through a 4 in pipe with 0.5 in diameter and a 0.25 in orifice. This flow likely defies the assumption of axisymmetric flow

did not converge well.

Simply by solving Equation 2.4, it would be expected that the orifice size is the only contributing factor to shaker performance. While the forces given above for varying pipe lengths and diameters are not exactly the same, their differences may be accounted for by questioning the underlying assumption of axisymmetric flow. This is especially true for simulations with the 4 in length and orifice sizes of at least 0.25 in as can be seen in Figure 3.8. However, it can be seen in Figure 3.1 that this was not a problem for the longer and wider Pipe sizes. Despite this lack of axisymmetry, the differences in shaker thrust were trivial in comparison with the differences due to orifice size. Thus, orifice size was the only Pipe characteristic varied in the up-scaling simulation.

The up-scaling simulation was run by solving the mass that could be shaken within a window of 18.5 Hz and 21.5 Hz for varying wall stiffness and orifice diameter. This was accomplished by iteratively adjusting the mass for each orifice size and stiffness combination and then running the

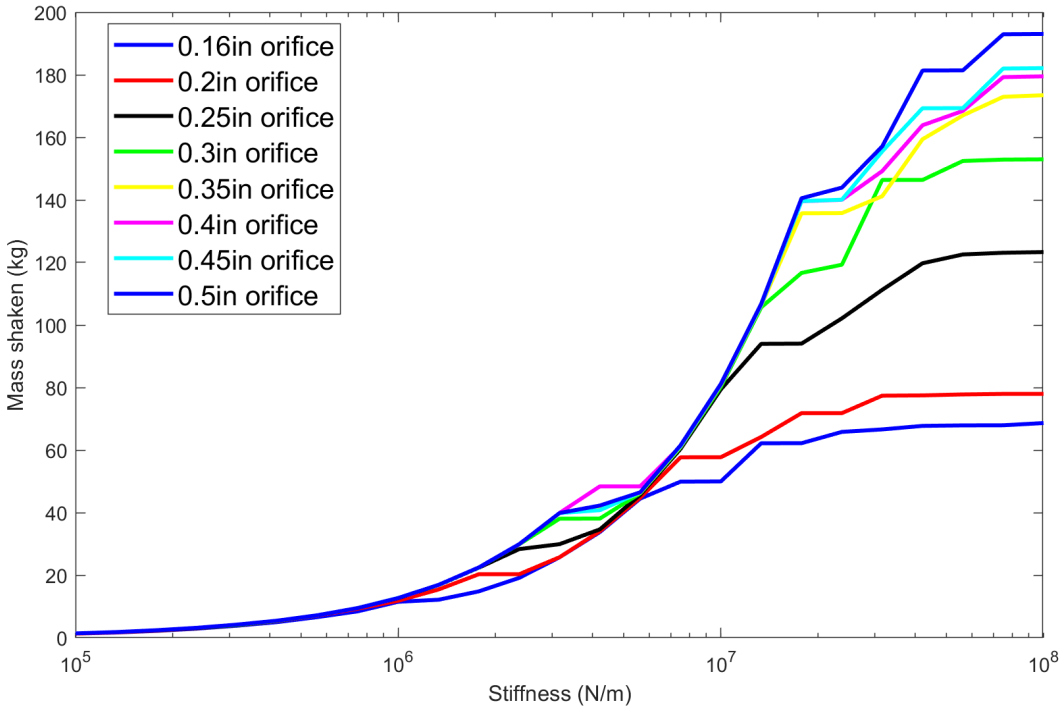

Figure 3.9: The amount of mass that can be shaken at 1mm and 20Hz as it varies with wall stiffness and orifice size

osc_motion function. Then the resulting shaker motion was put through a FFT, where the shaking frequency was determined for the case. If outside of the desired range, the mass was adjusted and the calculation was run again. Thus the simulation proved to be computationally taxing. In order to slightly decrease the computational cost of the simulation, the mass adjustments were made to be dynamic and based on the current stiffness value being analyzed. However, this had only minor effects on computational cost.

It can clearly be seen that at higher stiffnesses, the amount of weight that can be shaken begins to plateau. This shows that any stiffness value above 10^8 can be treated as a rigid wall for this system, and will provide no more benefit.

The up-scaling simulation was run with the expectation that there would be two shakers on the membrane unit. This was a design consideration from the start, as having two shakers would prevent imbalance on the centrifuge as it turned.

Table 3.4: Flow required for each orifice size in the up-scaling simulation

Orifice Size [in]	**Flow Required** [m^3/s]	**Force per Shaker** [N]	**Flow Required per shaker** [gpm]	**Force per Shaker** [lbf]
0.16	0.00049	27.13	7.78	6.10
0.2	0.00078	37.95	12.30	8.53
0.25	0.0013	61.01	20.26	13.72
0.3	0.0017	75.26	27.39	16.92
0.35	0.0022	85.67	34.42	19.26
0.4	0.0025	87.48	39.63	19.67
0.45	0.0029	89.58	45.97	20.14
0.5	0.0033	94.64	52.31	21.28

Figure 3.9 shows the amount of mass that can be shaken at the proper dynamic characteristics (1 mm, 20 Hz) within a tolerance of 1.5 Hz. This plot is semi-logarithmic, with the y axis varying linearly and the x axis varying logarithmically. It is important to note that at the smaller stiffness values, the shaker was far less likely to remain within the 1 mm amplitude set at the beginning. This problem was overlooked for two reasons. First, the simulation was based on oscillating frequency (which is the driving variable in membrane fouling control), it was deemed more important to keep the frequency within its proper tolerances. This amplitude issue is basically non-existent at higher stiffness values as well. Second, since this was a simulation for scaling up, the value it provides can be found in the higher end of the stiffness range. Since the problem only persisted on the low end, no changes were made to the model.

As the orifice size increases, it is clear to see that the flow requirements grow to be beyond the level of acceptable flow in a full system. For a full system, it would be difficult for the centrifuge to purify water reliably with the flow requirement of any orifice size above 0.25 in. Because CRO is useful with low recovery rates, however, it is plausible that an orifice size of 0.25 in or below would be achievable.

3.2 Experimentation

Due to the necessity for running tests within the confines of the shielding curtain, pictures of the tests themselves were not able to clearly show what was happening behind the curtain. Thus, detailed explanation will follow of the results.

The preliminary test of simply attaching the shaker to the hose and letting it run was performed as a simple proof to show that the jet is capable of providing sufficient force in the experiment setup. Since the shaker was not constrained by the end plates or shaker base, safety was a major consideration for this test. So, a low-pressure experiment was performed instead. The setup for this test can be seen in Figure 3.10.

The mass of the shaker was measured to be 2.89 kg before weights were added to simulate the full membrane unit. This brought the force of gravity on the shaker to 28.35 N. The pressure fed to the shaker was decreased to 300 psi for the sake of safety. The angle measured by the shaker was found to be roughly 15°. Plugging this into Equation 2.12 brought the force from the water jet to 7.34 N.

In order to determine if the shaker was providing the thrust as anticipated, a 300 psi simulation was performed as well. To see a breakdown of how the force was determined for this simulation, please refer to Section 2.2.1. The force for this simulation was found to be 10.91 N, which was higher than the force solved for based on the shaker angle. The difference in force values is likely due to the resistance of the hose to move. While the hose is flexible within a small range, its bending stiffness increases above 10°. Since this particular test was merely a proof of concept, further tests were not performed.

Next, the shaker was assembled with the end plates, though left off of the shaker base, in order to test shaft alignment. The shaker slid very easily on the linear bearings, showing there was no alignment problem between the shaker and the end plates.

Next, the shaker was attached to the hose, placed into the plates, and attached to the base. Once fully installed on the rig, the shaker became difficult to move. At the beginning of each run, the shaker was pushed to one of the extremes so that it would be in the FOFC position. The flow

Figure 3.10: Shaker hanging by the hose, before the preliminary flow test

through the system was measured to reach up to 6.5 gpm at full flow, which was lower than the simulated 7.7 gpm. When running the full 800 psi water through the shaker at 6.5 gpm, the force of the jet was not able to move the shaker at all. The lubrication on the bearings was increased by using Lithium soap based grease (as suggested by the bearing manufacturer), but this had little to no effect on the shaker. The cause of this was narrowed down to some potential misalignment upon final installation. It is believed that the misalignment is due to the overall dimensions of the end plates having a looser tolerance than acceptable for the project. When re-machining the end plates, it will be important to measure the outer holes (those that attach to the shaker base) from the center hole (through which the Plug moves) instead of measuring them from their outside edges as was done previously. Re-machining and assembly will be required in order to determine if it is, in fact, the end plates, or other components, such as the support flanges, need replacement as well.

It was also found that the Plug was very easy to move from side to side in the Pipe even at full pressure. This validated the pressure calculations from section 3.1.1.

Additionally, it was found that there was a significant amount of oxidation throughout the rig, as depicted in Figures 3.11 and 3.12. This was expected for certain parts of the rig, such as the Pipe and end caps, but it was more pervasive than previously anticipated. Due to the constant presence of water in the system, it is recommended that a water-driven shaker be made entirely of

Figure 3.11: Oxidation on the inside of the Pipe and end cap

stainless steel, aluminum, and other non-oxidizing materials. While the amount of rust seen in this experiment is acceptable for the test rig, it would lead to problems if run continually.

Figure 3.12: Oxidation on the outside of the linear bearings

4. SUMMARY AND CONCLUSIONS

The Plug-and-Pipe method was found to provide sufficient shaking for a 28 kg mass based on mathematical models. These CFX model was performed so that the momentum residuals in the simulation were below 10^4, which was deemed accurate enough to describe the system adequately. The only design factor that had a significant effect on the amount of force the shaker would release was the diameter of the orifice. Based on the simulations, it was found that the friction force allowable for the shaker system can not exceed 4.5% of the total weight of the mass being shaken. Friction beyond this value led to overdamped vibration. The driving force only acts on the shaker at the position extremes of its vibration, so in the full system, a method of holding the shaker in place during the ramp-up of the centrifuge is required.

For scaling the shaker up to large-scale CRO units, a breakdown of the amount of mass that can be shaken per orifice size across a range of wall stiffness values was presented. It was found that for this system, a stiffness of $10^8\mathrm{N/m}$ was the point at which the wall became essentially rigid. This means that, beyond $10^8\mathrm{N/m}$, increasing the stiffness will have no effect on the amount of mass that can be shaken. The up-scaling figure can be used as a guide for future work in the area of passive vibration for CRO systems.

The flow measured through the system was found to be 6.5 gpm, which was lower than the simulated flow of 7.7 gpm. This is likely due to the fact that the water was being pulled from a reservoir below the pump. In the future it is recommended to add a second reservoir above the pump that the flow can be pulled from, as well as a small pump which can transport water from the lower reservoir (which collects the water sprayed by the shaker) and the upper reservoir. The experiment rig seemed to have a problem with shaft alignment upon final installation on the rig. It seems that the hold placement on the end plates and support flanges were not within tolerance of the system. The end plates will have to be re-machined based on the proper specs. This time, however, instead of measuring the outer holes based on their relation to the sides of the plate, they will need to be measured based on their relation to the center hole through which the Plug will

travel. Finally, for the shaker to be implemented in a fully functioning CRO unit, it will need to be made of entirely non-oxidizing materials, as the constant presence of water could be a detriment to the shaker otherwise.

REFERENCES

[1] Food, A. Organization, and U. N. Water, "Coping with water scarcity: Challenge of the twenty-first century." Web, 2007.

[2] U. N. Development, "Human development report 2006." Web, 2006.

[3] C. for International Earth Science Information Network at Columbia University, "Percentage of total population living in coastal areas." Web, 2007.

[4] C. for International Earth Science Information Network at Columbia University, "Percentage of population in proximity to the coast." Web, 2010.

[5] C. for International Earth Science Information Network at Columbia University, "Coastal proximity zones." Web, 2007.

[6] T. Beacham and F. Towler, "Rotary, oscillating, and reciprocating seals," *Industrial Lubrication and Tribology*, vol. 2, no. 3, pp. 12–15, 1950.

[7] I. C. Karagiannis and P. G. Soldatos, "Water desalination cost literature: review and assessment," *Desalination*, vol. 223, pp. 448–456, December 2008.

[8] P. Wild, G. Vickers, and N. Djilali, "The fundamental principles and design considerations for the implementation of centrifugal reverse osmosis," *Proceedings of the Institution of Mechanical Engineers, Part E: Journal of Process Mechanical Engineering*, 1997.

[9] A. Berman, "Laminar flow in channels with porous walls," *Journal of Applied Physics*, vol. 24, pp. 1232–1235, September 1953.

[10] R. Singh and R. Laurence, "Influence of slip velocity at a membrane surface on ultrafiltration performance-i," *International Journal of Heat and Mass Transfer*, vol. 22, pp. 721–729, May 1979.

[11] S. Chellam, M. Wiesner, and C. Dawson, "Slip at a uniformly porous boundary: effect on fluid flow and mass transfer," *Journal of Engineering Mathematics*, vol. 26, pp. 481–492, November 1992.

[12] B. Culkin and A. Armando, "New separation system extends the use of membranes," *Filtration and Separation*, vol. 29, pp. 376–378, October 1992.

[13] R. Bian, K. Yamamoto, and Y. Watanabe, "The effect of shear rate on controlling the concentration polarization and membrane fouling," *Desalination*, vol. 131, pp. 225–236, December 2000.

[14] K. Takata, K. Yamamoto, R. Bian, and Y. Watanabe, "Removal of humic substances with vibratory shear enhanced processing membrane filtration," *Desalination*, vol. 117, pp. 273–282, September 1998.

[15] O. Akoum, M. Jaffrin, L. Ding, P. Paullier, and C. Vanhoutte, "An hydrodynamic investigation of microfiltration and ultrafiltration in a vibrating membrane module," *Journal of Membrane Science*, vol. 197, pp. 37–52, 2002.

[16] M. Jaffrin, L. Ding, O. Akoum, and A. Brou, "A hydrodynamic comparison between rotating disk and vibratory dynamic filtration systems," *Journal of Membrane Science*, vol. 242, pp. 37–52, October 2004.

[17] W. Shi and M. Benjamin, "Fouling of ro membranes in a vibratory shear enhanced filtration process (vsep) system," *Journal of Membrane Science*, vol. 331, pp. 11–20, April 2009.

[18] W. Shi and M. Benjamin, "Effect of shear rate on fouling in a vibratory shear enhanced processing (vsep) ro system," *Journal of Membrane Science*, vol. 366, pp. 148–157, January 2011.

[19] X. Su, W. Li, A. Palazzolo, and S. Ahmed, "Concentration polarization and permeate flux variation in a vibration enhanced reverse osmosis membrane module," *Desalination*, vol. 433, pp. 75–88, May 2018.

[20] ANSYS, "Ansys help documents." Web, 2015.

[21] J. A. Lock, “The flow of water through small orifices (unpublished master’s thesis),” *Texas A&M University College of Engineering Master’s Collection*, July 1954.

[22] B. R. Corporation, “External gear pumps, series f.” Web, 2011.

APPENDIX A

SOLIDWORKS AND ANSYS MODELS

This appendix contains the details of the models used in this project.

A.1 SolidWorks Drawings

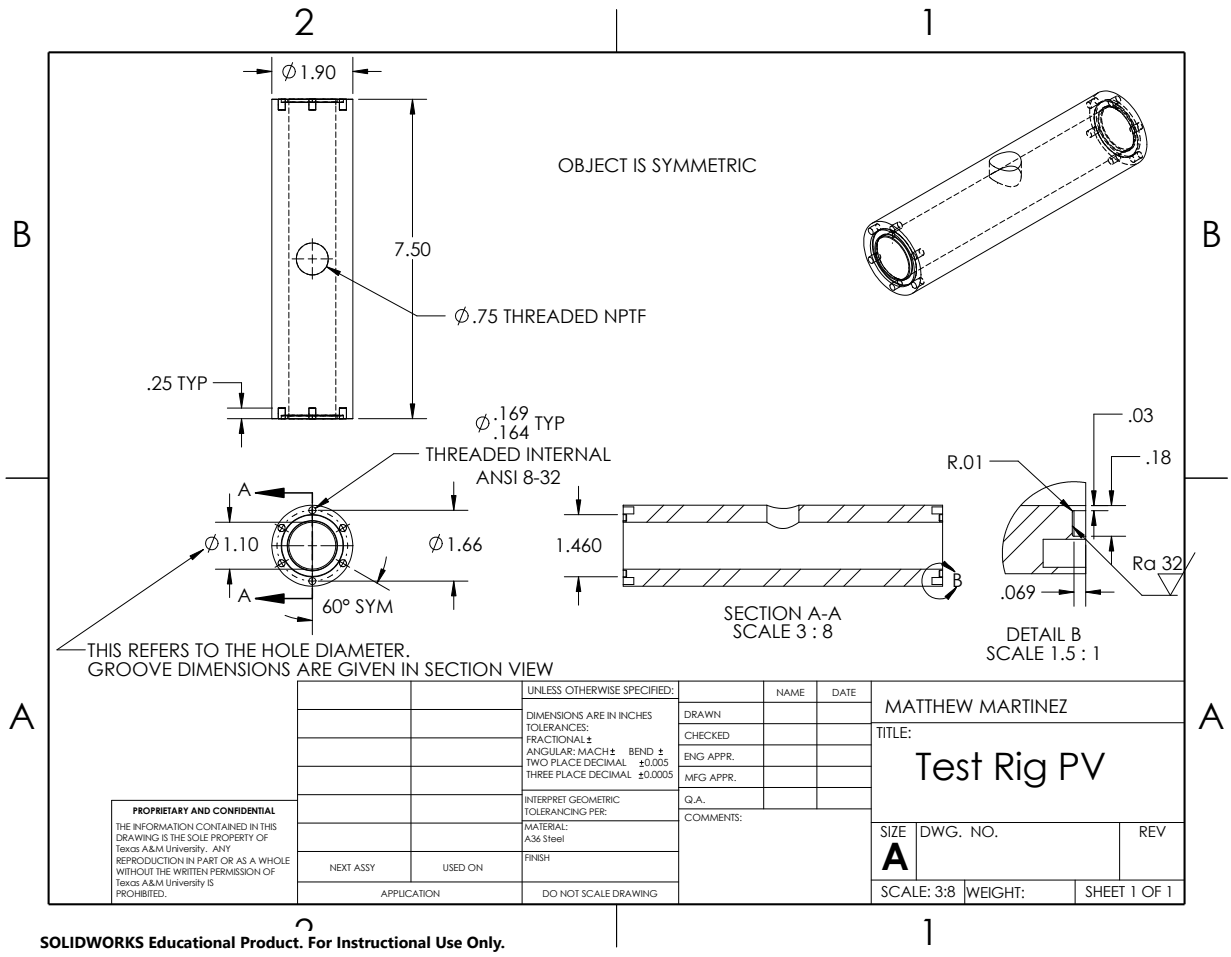

Figure A.1: Dimensioned drawing of the Pipe

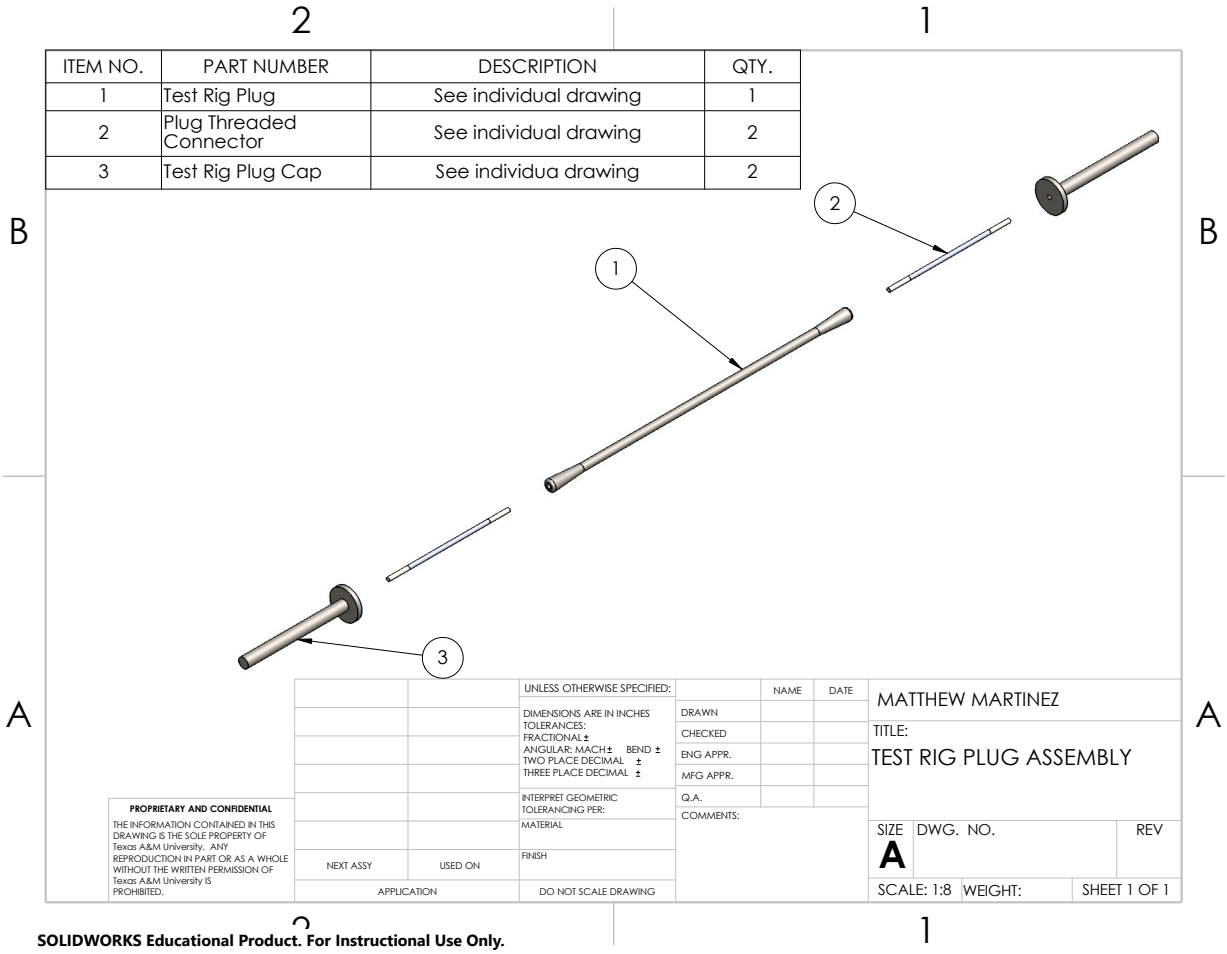

Figure A.2: Drawing of the Plug assembly

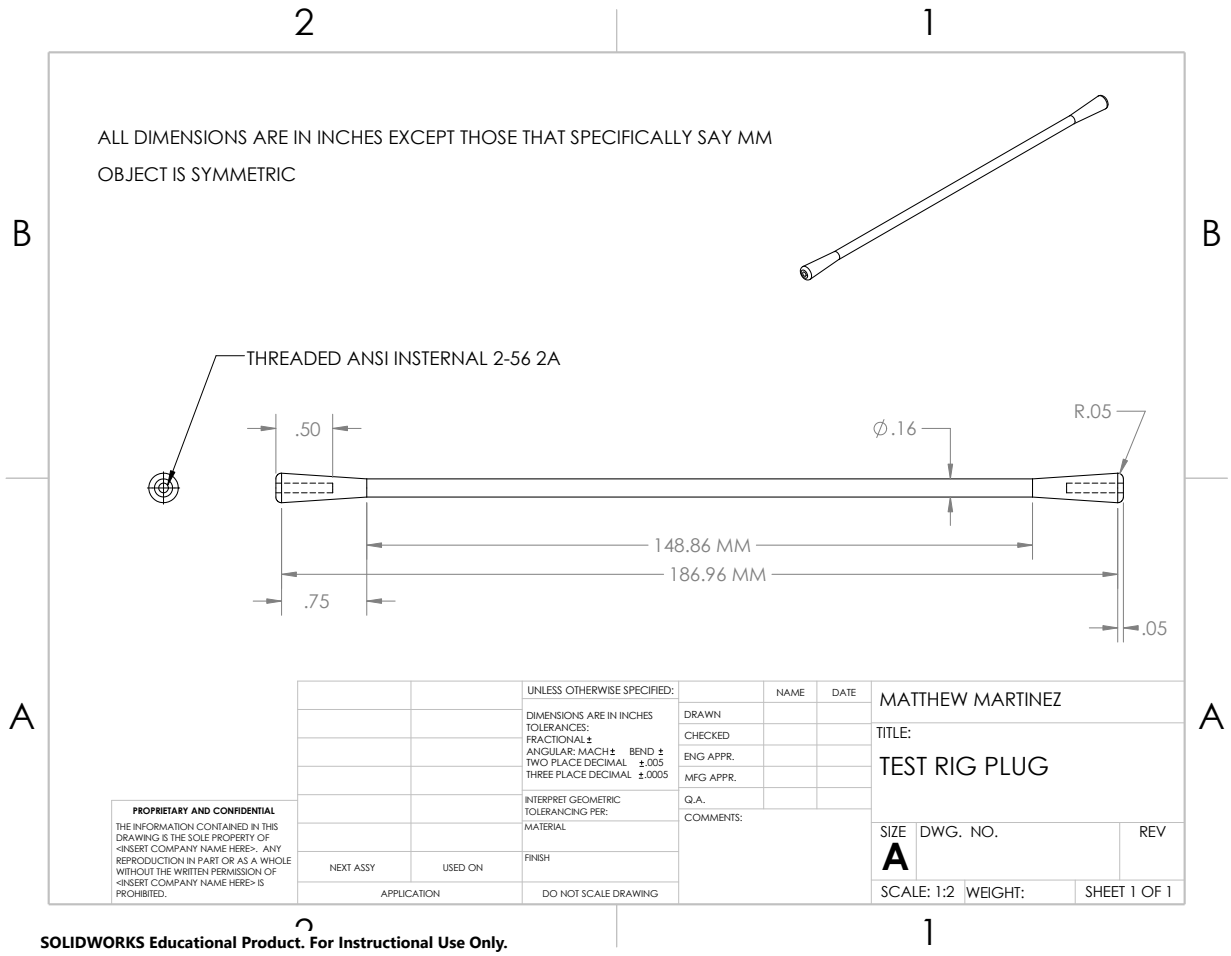

Figure A.3: Dimensioned drawing of the Plug body

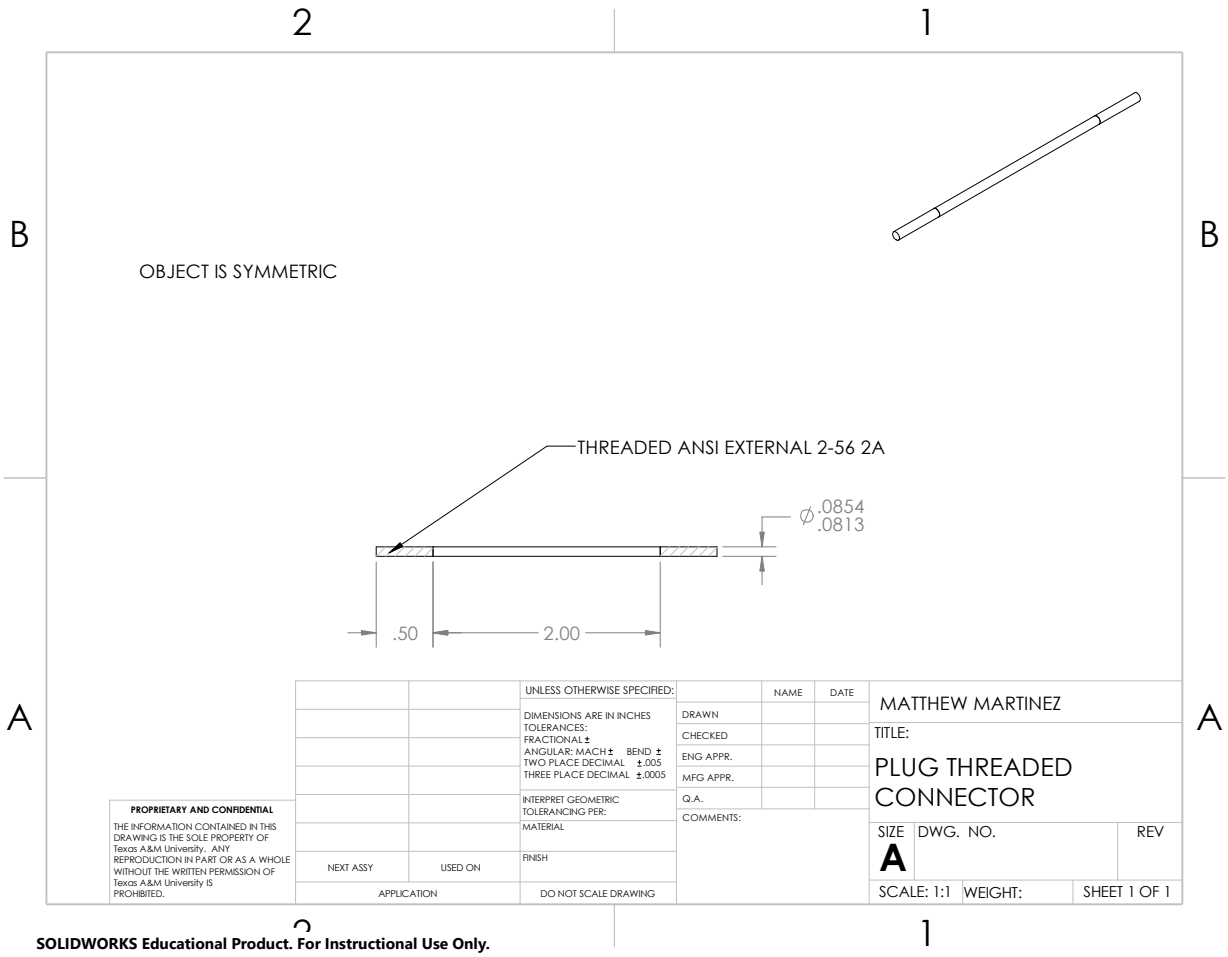

Figure A.4: Dimensioned drawing of the Plug threaded connectors

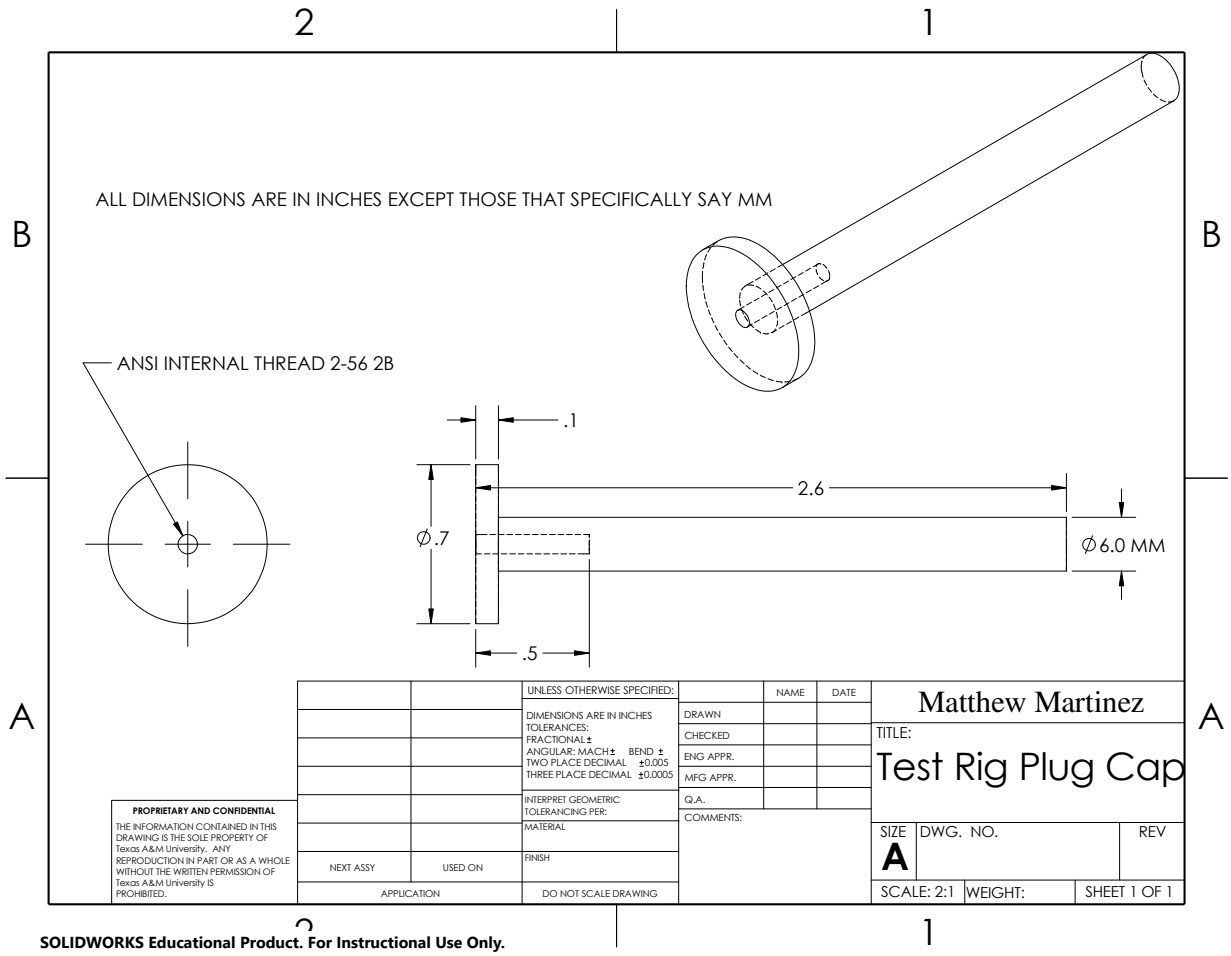

Figure A.5: Dimensioned drawing of the Plug caps

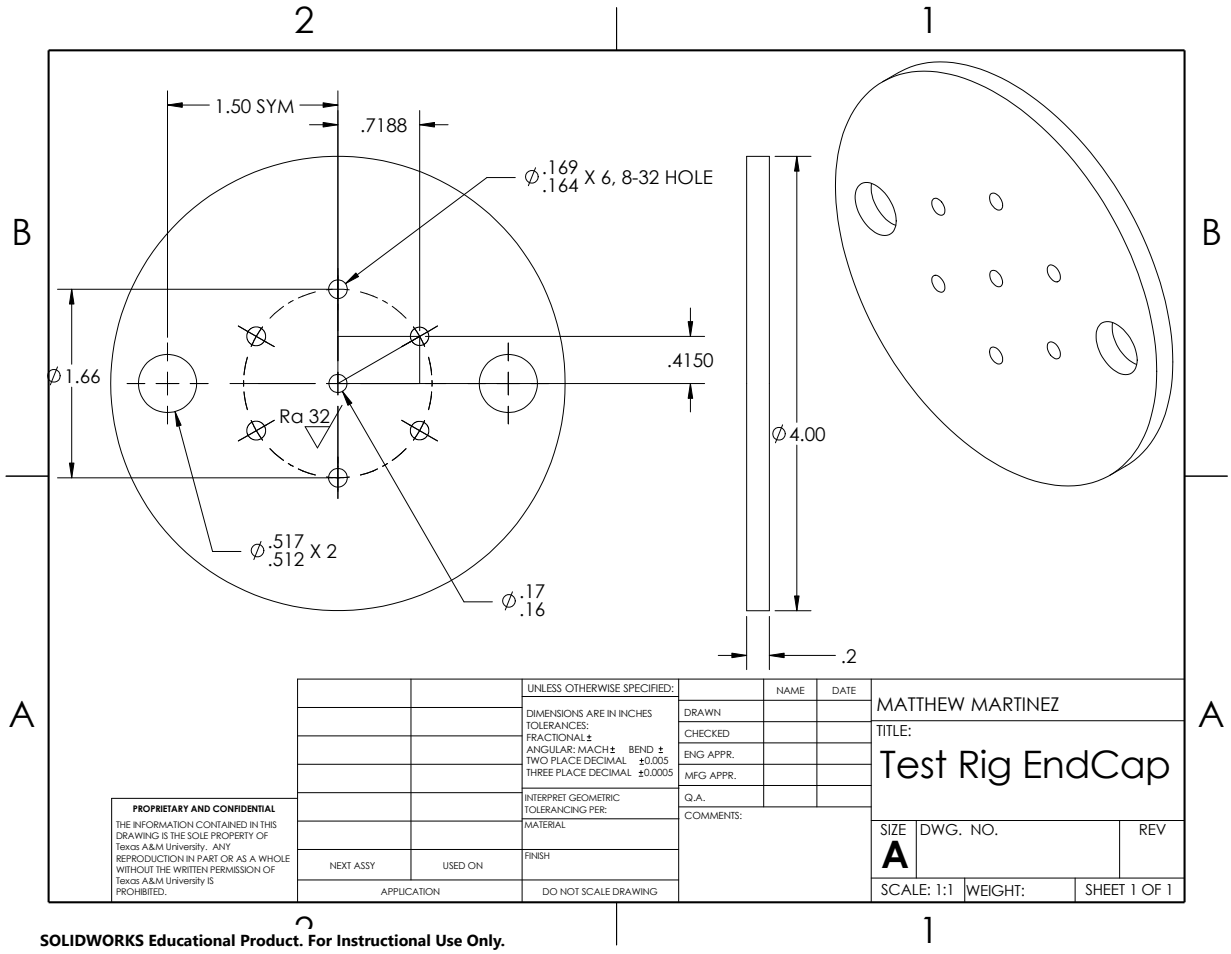

Figure A.6: Dimensioned drawing of the end caps

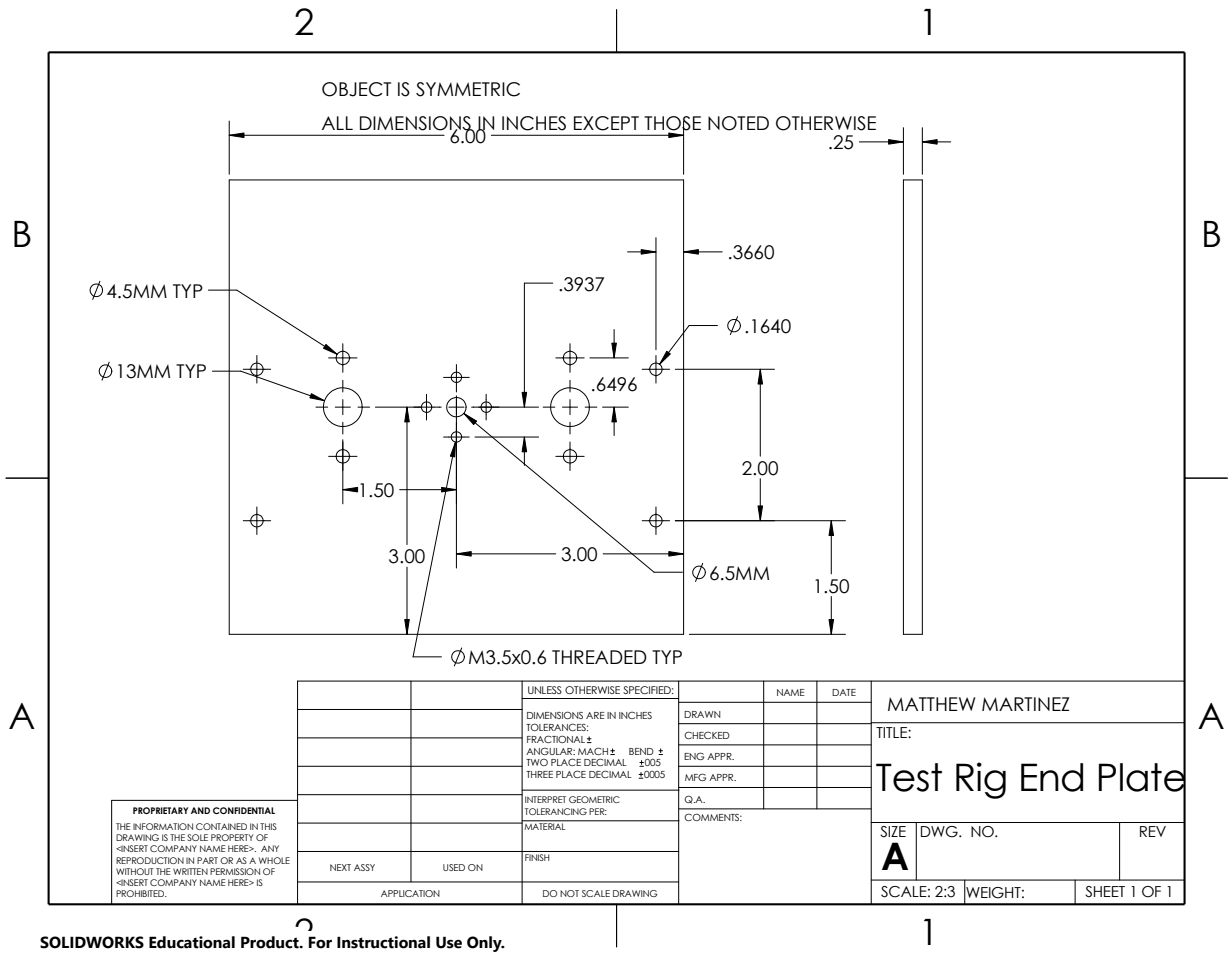

Figure A.7: Dimensioned drawing of the end plates

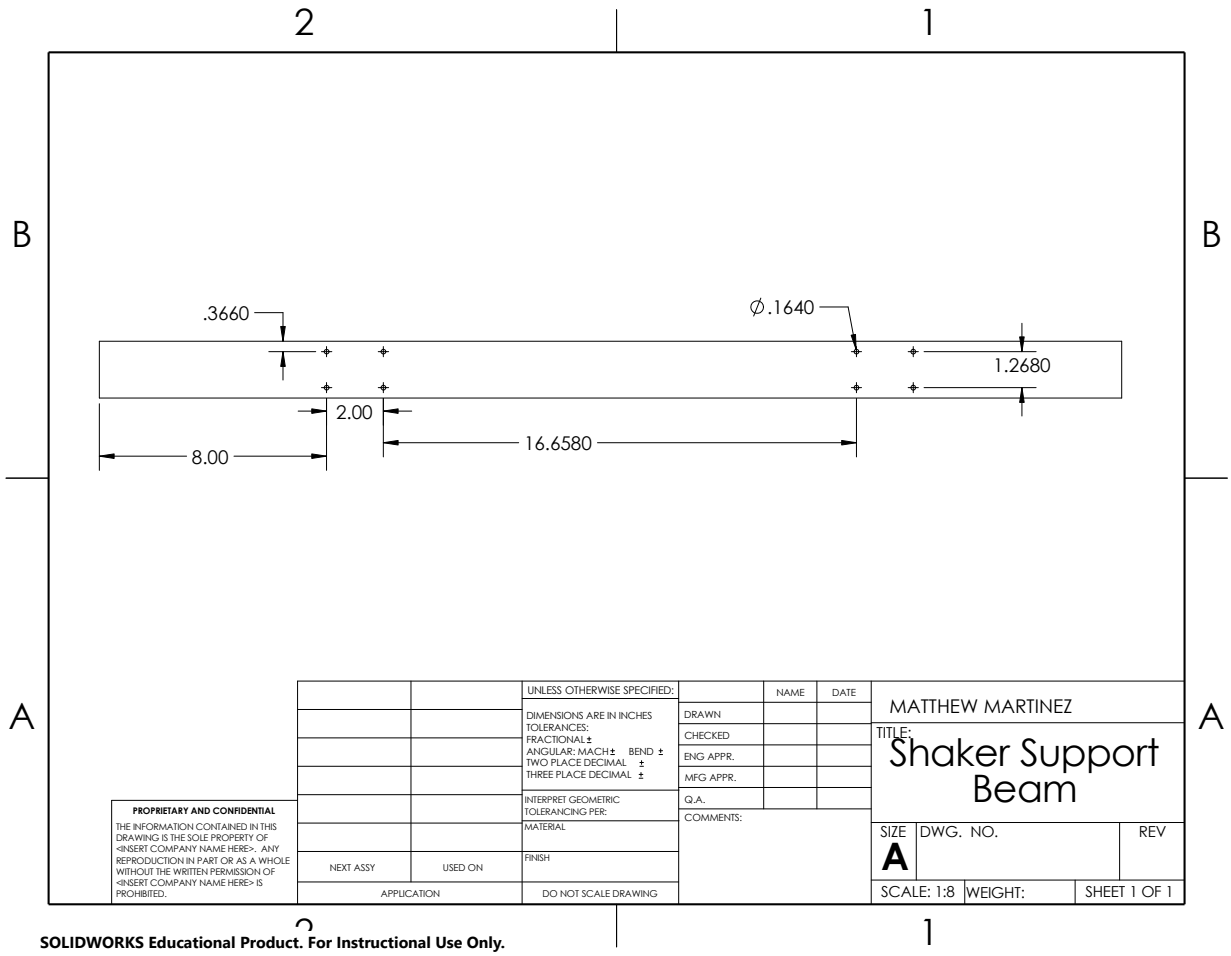

Figure A.8: Dimensioned drawing of the shaker support beams

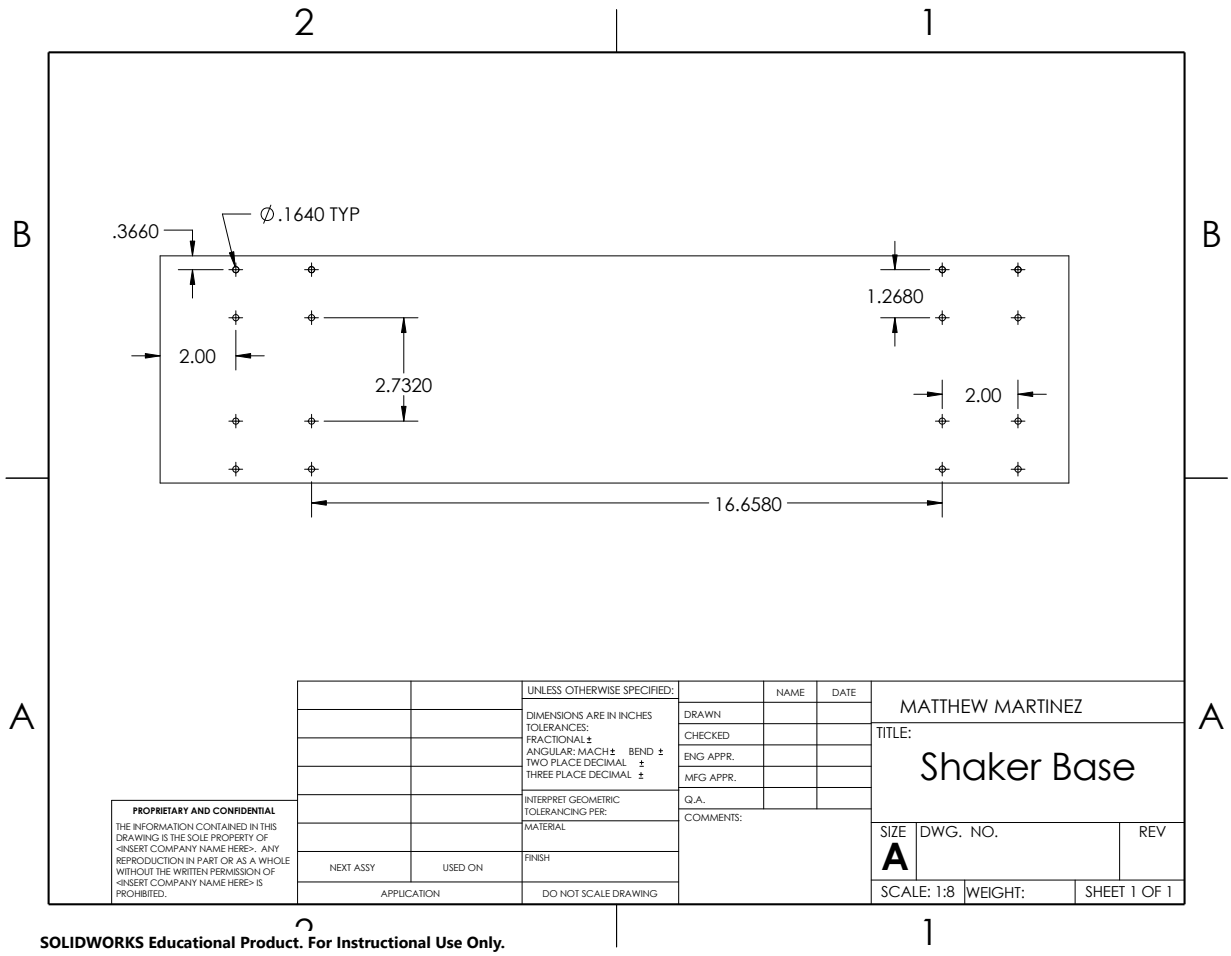

Figure A.9: Dimensioned drawing of the shaker base

A.2 ANSYS Simulations

Parameters for the mesh used in each of the CFX simulations.

Table A.1: ANSYS Meshing settings

Setting	**Option**
Size Function	Proximity and Curvature
Relevance Center	Medium
Max Face Size	Default
Mesh Defeaturing	Yes
Defeature Size	2.5E-06 m
Transition	Slow
Growth Rate	Default
Span Angle Center	Fine
Min Size	5.0E-06
Max Tet Size	Default
Curvature Normal Angle	Default
Proximity Min Size	5.0E-06
Num Cells Across Gap	Default
Proximity Size Function Sources	Faces and Edges
Check Mesh Quality	Yes, Errors
Target Skewness	Default
Smoothing	Medium
Mesh Metric	None
Use Automatic Inflation	None
Inflation Option	Smooth Transition
Transition Ratio	0.77
Maximum Layers	5
Growth Rate	1.2
Inflation Algorithm	Pre
View Advanced Options	No
Number of CPU's for Parallel Part Meshing	Program Controlled
Mesh Morphing	Disabled
Triangle Surface Mesher	Program Controlled
Topology Checking	No
Pinch Tolerance	Default
Generate Pinch on Refresh	No
Nodes	34039
Elements	179615

APPENDIX B

MATLAB CODE

This appendix contains the MATLAB code used in this project.

B.1 Velocity Distribution Calculation

First, we have the script $Size\_Optimization\_Curve\_Fit\_1mm$, which stored the discrete velocities which were to be put into MATLAB's $cftool$.

```
% ALL DATA ARE FROM FULLY OPEN FULLY CLOSED SIMULATIONS WITH ONLY 1MM GAP
%% This section for 4in 0.5inD, 0.16 orifice, 0.085 blocked optimmization ...
    attempt
x4 = [0.00109 0.0012 0.0013 0.0014 0.0015 0.0016 0.0017 0.0018 0.0019 ...
    0.002 0.002032];

%% This section for 0.2inO 0.085B comparisons
x02 = [0.00109 0.0012 0.0014 0.0016 0.0018 0.002 0.0021 0.0022 0.0023 ...
    0.0024 0.0025 0.00254];
%% This section for 7in 0.5D 0.085B comparisons
x016 = [0.00109 0.0012 0.0013 0.0014 0.0015 0.0016 0.0017 0.0018 0.0019 ...
    0.002 0.002032];
yL016 = [55.29 57.111 59.173 61.144 62.686 62.262 60.278 53.965 44.936 ...
    33.348 29.539];
yL02 = [42.913 45.329 49.245 52.771 56.386 56.876 56.320 51.835 45.644 ...
    36.325 23.967 19.730];
yL025 = [30.984 32.758 36.1 39.31 42.631 46.098 48.646 50.119 49.704 ...
    42.324 29.686 14.292];

%% This section for 4in 1.1D 0.085B comparisons
```

```
x025 = [0.00109 0.0012 0.0014 0.0016 0.0018 0.002 0.0022 0.0024 0.0026 ...
    0.0028 0.003 0.003175];
x035 = [0.00109 0.0012 0.0016 0.002 0.0024 0.0028 0.0032 0.0036 0.0038 ...
    0.004 0.0042 0.0044 0.004445];

%% This section for 7in 1.1D 0.085B comparisons
%This one for the full 1.1D, 0.16O, 0.085B
xfofc = [0.00109 0.0012 0.0013 0.0014 0.0015 0.0016 0.0017 0.0018 0.0019 ...
    0.002 0.002032];
yfofc = [63.582 64.54 64.963 66.162 66.814 66.894 64.962 58.705 49.918 ...
    35.444 30.744];
Velocity = [53.3756 56.2295 59.1962 61.5445 62.8178 61.626 60.2974 52.2877 ...
    42.1128 27.6163 22.9775];
Radius = [0.00109 0.0012 0.0013 0.0014 0.0015 0.0016 0.0017 0.0018 0.0019 ...
    0.002 0.002032];
Pressfofc = -1*[-1.70E+06 -1.77E+06 -1.85E+06 -1.97E+06 -2.18E+06 ...
    -2.47E+06 -2.91E+06 -3.21E+06 -3.48E+06 -3.21E+06 -3.11E+06];

% This one for the full 1.1D 0.16O 0.085B 300 psi case
yf016_300 = [34.5395 35.7365 36.4875 37.3478 38.3871 38.6041 38.2219 ...
    34.4649 27.7284 19.481 16.8093];
%These for the rest
yf02 = [48.958 49.719 52.507 55.459 55.988 52.386 48.532 44.821 40.304 ...
    32.231 24.471 21.552];
yf025 = [41.348 42.22 43.544 45.564 48.133 51.233 53.672 55.123 54.154 ...
    47.113 32.138 15.257];
x03 = [0.00109 0.0012 0.0016 0.002 0.0024 0.0026 0.0028 0.003 0.0032 ...
    0.0034 0.0036 0.00381];
yf03 = [37.752 38.23 38.648 42.711 48.162 50.32 50.879 50.267 46.975 39.24 ...
    27.915 10.224];
yf035 = [32.351 32.559 33.656 35.621 39.938 44.723 47.008 44.765 40.52 ...
    33.475 23.503 12.773 9.839];
```

```
x04 = [0.00109 0.0012 0.0016 0.002 0.0024 0.0028 0.0032 0.0036 0.004 ...
    0.0044 0.0046 0.0048 0.00508];
x045 = [0.00109 0.0012 0.0016 0.002 0.0024 0.0028 0.0032 0.0036 0.004 ...
    0.0044 0.0048 0.0052 0.0054 0.0056 0.005715];
x05 = [0.00109 0.0012 0.0016 0.002 0.0024 0.0028 0.0032 0.0036 0.004 ...
    0.0044 0.0048 0.0052 0.0056 0.0058 0.006 0.0062 0.00635];
yf04 = [23.837 24.3536 26.3759 29.6559 32.6991 37.0473 40.5298 42.2034 ...
    39.7441 33.0418 27.8782 21.2277 9.4223];
yf045 = [18.5753 19.137 21.907 24.102 27.588 31.01 34.434 37.332 38.62 ...
    36.264 31.48 23.255 18.667 12.335 7.828];
yf05 = [16.1677 16.682 18.665 20.789 23.671 26.333 29.824 32.828 34.779 ...
    36.114 34.363 30.366 24.102 20.417 15.977 10.938 6.357];
yobe025 = [36.3456 36.9166 36.9908 39.1532 39.2798 38.0976 32.4937 26.0715 ...
    17.4081 9.34665 6.33016];
yobe075 = [50.9566 53.4985 55.7512 58.1311 59.2283 59.1999 56.1982 48.0885 ...
    39.9569 28.8093 25.1683];
yobe05L = [44.5075 46.3436 48.3029 51.3876 53.5089 54.7794 50.1423 44.8165 ...
    33.9346 20.9825 15.9272];
yobe05R = [43.0804 45.8447 48.2248 51.4253 54.0456 52.9854 50.7683 43.6374 ...
    32.2094 19.6869 15.2894];



%% This section for the 7in 0.75D 0.085B comparisons
y775016 = [56.562 58.387 59.496 60.846 62.596 63.479 61.911 56.664 44.364 ...
    26.214 19.688];
y77502 = [48.789 50.141 52.628 55.294 58.011 59.556 58.285 54.75 46.764 ...
    37.262 22.613 17.249];
y775025 = [40.059 40.987 43.182 45.232 47.85 51.1 55.54 54.922 53.476 ...
    46.064 32.291 15.252];
y77503 = [27.557 28.753 34.899 41.202 47.644 49.939 50.728 49.147 46.123 ...
    39.407 26.652 9.648];
```

```
y775035 = [23.392 24.091 27.372 32.302 38.223 43.117 46.138 44.174 39.974 ...
    32.576 24.587 11.131 8.219];
%% This section for the 4in 1.1D 0.085B comparisons
y411016 = [56.807 58.541 59.535 60.996 62.281 64.164 61.748 57.078 45.621 ...
    30.476 25.663];
y41102 = [48.66 50.193 52.466 55.175 58.216 59.822 58.252 54.402 47.25 ...
    36.727 24.8 19.846];
y411025 = [39.399 40.743 42.829 45.272 47.718 50.533 52.957 54.548 54.32 ...
    46.085 32.497 16.53];
y41103 = [31.095 31.985 35.792 40.36 46.55 48.774 50.035 50.216 47.211 ...
    39.238 27.811 12.602];
y411035 = [24.538 25.004 28.215 32.623 38.342 43.146 45.754 43.777 39.901 ...
    33.171 24.656 13.259 10.655];
%% This section for the 4in 0.75D 0.085B comparisons
y475016 = [56.484 58.291 59.426 61.188 62.407 63.188 61.576 55.825 44.35 ...
    30.592 25.953];
y47502 = [46.338 48.414 51.746 54.751 58.235 59.259 57.604 52.422 45.527 ...
    36.925 24.261 19.114];
y475025 = [34.54 36.384 39.705 43.04 48.22 49.65 51.968 53.385 52.349 ...
    46.05 32.044 19.335];
y47503 = [27.833 29.325 34.562 41.181 48.504 50.996 52.341 52.18 48.942 ...
    41.085 28.763 13.909];
y47035 = [23.253 24.156 27.6 32.113 37.959 42.847 45.472 43.701 39.391 ...
    33.317 23.727 11.491 8.636];
%% This section for the 4in 0.5D 0.085B comparisons
y45016 = [55.384 57.508 59.142 60.979 61.838 60.262 54.987 49.736 38.417 ...
    26.434 22.57];
y4502 = [41.3433 44.2066 48.1897 51.096 53.319 54.949 52.669 49.194 43.721 ...
    35.24 28.887 20.401];
y45025 = [30.001 32.568 36.901 40.949 44.794 47.897 50.921 52.757 52.417 ...
    47.494 34.96 18.855];
```

Next, the values were put into $cftool$ and the velocity distributions were put into $Force\_Balance\_Orifice\_Si$

as shown below

```
%% Global Variables
global Ff16 qf16 Ff2 qf2 Ff25 qf25 Ff3 qf3 Ff35 qf35 F42 q42 FL16 qL16 FL2 ...
    qL2 FL25 qL25 F41016 q41016 F4102 q4102 F41025 q41025 F4103 q4103 ...
    F41035 q41035 ...
     F775016 q775016 F77502 q77502 F775025 q775025 F77503 q77503 F775035 ...
         q775035 F475016 q475016 F47502 q47502 F475025 q475025 F47503 ...
         q47503 F475035 q475035 ...
     Ff16_300 qf16_300
r1 = 0.00109;
r22 = 0.00254;
r216 = 0.002032;
r225 = 0.003175;
r23 = .00381;
r235 = .004445;
r24 = .00508;
r245 = .005715;
r25 = .00635;
rho = 1000;
%% This section for the pressure at the orifice for the Full 1.1D 0.16O ...
    0.085B FOFC FINAL
p1f16 = @(r) pi()*r.*(-1.954e19*r.^4 + 1.134e17*r.^3 - 2.409e14*r.^2 + ...
    2.239e11*r - 7.535e7);
Pf16 = integral(p1f16, r1, r216);

%% This section for the full 1.1D 0.16O 0.085B FOFC FINAL
v1f16f = @(r) 2*pi()*r.*(3.856e13*r.^4 - 3.492e11*r.^3 + 9.511e8*r.^2 - ...
    1.012e6*r + 424.2).^2;
f1f16f = integral(v1f16f, r1, r216);
Ff16f = f1f16f*rho
vf16f = @(r) 2*pi()*r.*(3.856e13*r.^4 - 3.492e11*r.^3 + 9.511e8*r.^2 - ...
```

```
    1.012e6*r + 424.2);
qf16f = integral(vf16f, r1, r216)
%% This section for the full 1.1D 0.16O 0.085 OBE 0.25mm
v1obe1625 = @(r) 2*pi()*r.*(2.184e14*r.^4 - 1.404e12*r.^3 + 3.258e9*r.^2 - ...
    3.253e6*r + 1221).^2;
f1obe1625 = integral(v1obe1625, r1, r216);
Fobe1625 = f1obe1625*rho;
vobe1625 = @(r) 2*pi()*r.*(2.184e14*r.^4 - 1.404e12*r.^3 + 3.258e9*r.^2 - ...
    3.253e6*r + 1221);
qobe1625 = integral(vobe1625, r1, r216);
%% This section fo rthe full 1.1D 0.16O 0.085 OBE 0.5mm Left side
v1obe165L = @(r) 2*pi()*r.*(1.202e14*r.^4 - 8.738e11*r.^3 + 2.2e9*r.^2 - ...
    2.314e6*r + 915).^2;
f1obe165L = integral(v1obe165L, r1, r216);
Fobe165L = f1obe165L*rho;
vobe165L = @(r) 2*pi()*r.*(1.202e14*r.^4 - 8.738e11*r.^3 + 2.2e9*r.^2 - ...
    2.314e6*r + 915);
qobe165L = integral(vobe165L, r1, r216);
%% This section fo rthe full 1.1D 0.16O 0.085 OBE 0.5mm Right side
v1obe165R = @(r) 2*pi()*r.*(1.399e14*r.^4 - 9.79e11*r.^3 + 2.397e9*r.^2 - ...
    2.462e6*r + 948.9).^2;
f1obe165R = integral(v1obe165R, r1, r216);
Fobe165R = f1obe165R*rho;
vobe165R = @(r) 2*pi()*r.*(1.399e14*r.^4 - 9.79e11*r.^3 + 2.397e9*r.^2 - ...
    2.462e6*r + 948.9);
qobe165R = integral(vobe165R, r1, r216);
%% This section for the full 1.1D 0.16O 0.085 OBE 0.75mm
v1obe1675 = @(r) 2*pi()*r.*(1.374e14*r.^4 - 9.299e11*r.^3 + 2.219e9*r.^2 - ...
    2.233e6*r + 859).^2;
f1obe1675 = integral(v1obe1675, r1, r216);
Fobe1675 = f1obe1675*rho;
vobe1675 = @(r) 2*pi()*r.*(1.374e14*r.^4 - 9.299e11*r.^3 + 2.219e9*r.^2 - ...
    2.233e6*r + 859);
```

```
qobe1675 = integral(vobe1675, r1, r216);
%% Average velocity (for Reynold's calculation)
for ii = 1:50
    r_rey(ii) = (ii)*(r216-r1)/50 + r1;
    v_rey(ii) = -2.85e13*r_rey(ii)^4 +4.297e10*r_rey(ii)^3 + ...
        1.313e8*r_rey(ii)^2 - 2.961e5*r_rey(ii) + 215;
end

v_avg_rey = mean(v_rey);
%% This section for the full 1.1D 0.16O 0.085B 300psi FOFC
v1f16_300 = @(r) 2*pi()*r.*(3.025e12*r.^4 - 1.052e11*r.^3 + 3.876e8*r.^2 - ...
    4.875e5*r + 237.6).^2;
f1f16_300 = integral(v1f16_300, r1, r216);
Ff16_300 = f1f16_300*rho
vf16_300 = @(r) 2*pi()*r.*(3.025e12*r.^4 - 1.052e11*r.^3 + 3.876e8*r.^2 - ...
    4.875e5*r + 237.6);
qf16_300 = integral(vf16_300, r1, r216)
%% This section for the full 1.1D, 0.2O, 0.085B FOFC
v1f2 = @(r) 2*pi()*r.*(1.456e13*r.^4 - 1.275e11*r.^3 + 3.599e8*r.^2 - ...
    4.021e5*r + 204.2).^2;
f1f2 = integral(v1f2, r1, r22);
Ff2 = f1f2*rho
vf2 = @(r) 2*pi()*r.*(1.456e13*r.^4 - 1.275e11*r.^3 + 3.599e8*r.^2 - ...
    4.021e5*r + 204.2);
qf2 = integral(vf2, r1, r22)
%% This section for the full 1.1D 0.25O 0.085B FOFC
v1f25 = @(r) 2*pi()*r.*(-8.466e12*r.^4 + 4.879e10*r.^3 - 9.507e7*r.^2 + ...
    8.081e4*r + 15.2).^2;
f1f25 = integral(v1f25, r1, r225);
Ff25 = f1f25*rho
vf25 = @(r) 2*pi()*r.*(-8.466e12*r.^4 + 4.879e10*r.^3 - 9.507e7*r.^2 + ...
    8.081e4*r + 15.2);
qf25 = integral(vf25, r1, r225)
```

```
%% This section for the full 1.1D 0.3O 0.085B FOFC
v1f3 = @(r) 2*pi()*r.*(-2.511e12*r.^4 + 1.294e10*r.^3 - 1.334e7*r.^2 - ...
    8641*r + 50.16).^2;
f1f3 = integral(v1f3, r1, r23);
Ff3 = f1f3*rho
vf3 = @(r) 2*pi()*r.*(-2.511e12*r.^4 + 1.294e10*r.^3 - 1.334e7*r.^2 - ...
    8641*r + 50.16);
qf3 = integral(vf3, r1, r23)
%% This section for the full 1.1D 0.35O 0.085B FOFC
v1f35 = @(r) 2*pi()*r.*(-7.421e11*r.^4 + 2.446e9*r.^3 + 7.555e6*r.^2 - ...
    2.586e4*r + 49.81).^2;
f1f35 = integral(v1f35, r1, r235);
Ff35 = f1f35*rho
vf35 = @(r) 2*pi()*r.*(-7.421e11*r.^4 + 2.446e9*r.^3 + 7.555e6*r.^2 - ...
    2.586e4*r + 49.81);
qf35 = integral(vf35, r1, r235)
%% This section for the full 1.1D 0.4O 0.085B FOFC
v1f4 = @(r) 2*pi()*r.*(-1.501e11*r.^4 - 8.306e8*r.^3 + 1.105e7*r.^2 - ...
    1.99e4*r + 33.96).^2;
f1f4 = integral(v1f4, r1, r24);
Ff4 = f1f4*rho
vf4 = @(r) 2*pi()*r.*(-1.501e11*r.^4 - 8.306e8*r.^3 + 1.105e7*r.^2 - ...
    1.99e4*r + 33.96);
qf4 = integral(vf4, r1, r24)
%% This section for the full 1.1D 0.45O 0.085B FOFC
v1f45 = @(r) 2*pi()*r.*(-2.572e10*r.^4 - 1.16e9*r.^3 + 9.5e6*r.^2 - ...
    1.465e4*r + 25.12).^2;
f1f45 = integral(v1f45, r1, r245);
Ff45 = f1f45*rho
vf45 = @(r) 2*pi()*r.*(-2.572e10*r.^4 - 1.16e9*r.^3 + 9.5e6*r.^2 - ...
    1.465e4*r + 25.12);
qf45 = integral(vf45, r1, r245)
%% This section for the full 1.1D 0.5O 0.085B FOFC
```

```
v1f5 = @(r) 2*pi()*r.*(1.651e10*r.^4 - 1.254e9*r.^3 + 9.285e6*r.^2 - ...
    1.543e4*r + 23.97).^2;
f1f5 = integral(v1f5, r1, r25);
Ff5 = f1f5*rho
vf5 = @(r) 2*pi()*r.*(1.651e10*r.^4 - 1.254e9*r.^3 + 9.285e6*r.^2 - ...
    1.543e4*r + 23.97);
qf5 = integral(vf5, r1, r25)
%% This section for the Long (7in) 0.5D 0.16O 0.085B FOFC
v1L16 = @(r) 2*pi()*r.*(7.877e13*r.^4 - 5.883e11*r.^3 + 1.493e9*r.^2 - ...
    1.567e6*r + 639.7).^2;
f1L16 = integral(v1L16, r1, r216);
FL16 = f1L16*rho
vL16 = @(r) 2*pi()*r.*(7.877e13*r.^4 - 5.883e11*r.^3 + 1.493e9*r.^2 - ...
    1.567e6*r + 639.7);
qL16 = integral(vL16, r1, r216)
%% This section for the Long 0.5D 0.2O 0.085B FOFC
v1L2 = @(r) 2*pi()*r.*(-1.988e13*r.^4 + 9.26e10*r.^3 - 1.499e8*r.^2 + ...
    1.15e5*r + 4.094).^2;
f1L2 = integral(v1L2, r1, r22);
FL2 = f1L2*rho
vL2 = @(r) 2*pi()*r.*(-1.988e13*r.^4 + 9.26e10*r.^3 - 1.499e8*r.^2 + ...
    1.15e5*r + 4.094);
qL2 = integral(vL2, r1, r22)
%% This section for the long 0.5D 0.25O 0.085B FOFC
v1L25 = @(r) 2*pi()*r.*(-7.208e12*r.^4 + 4.191e10*r.^3 - 8.736e7*r.^2 + ...
    9.336e4*r - 10.97).^2;
f1L25 = integral(v1L25, r1, r225);
FL25 = f1L25*rho
vL25 = @(r) 2*pi()*r.*(-7.208e12*r.^4 + 4.191e10*r.^3 - 8.736e7*r.^2 + ...
    9.336e4*r - 10.97);
qL25 = integral(vL25, r1, r225)
%% This section for the 7in 0.75D 0.16O 0.085B FOFC
v1775016 = @(r) 2*pi()*r.*(-1.141e14*r.^4 + 5.176e11*r.^3 - 8.448e8*r.^2 + ...
```

```
    5.934e5*r - 95.51).^2;
f1775016 = integral(v1775016, r1, r216);
F775016 = f1775016*rho
v775016 = @(r) 2*pi()*r.*(-1.141e14*r.^4 + 5.176e11*r.^3 - 8.448e8*r.^2 + ...
    5.934e5*r - 95.51);
q775016 = integral(v775016, r1, r216)
%% This section for the 7in 0.75D 0.2O 0.085B FOFC
v177502 = @(r) 2*pi()*r.*(-3.376e13*r.^4 + 1.812e11*r.^3 - 3.516e8*r.^2 + ...
    3.038e5*r - 51.45).^2;
f177502 = integral(v177502, r1, r22);
F77502 = f177502*rho
v77502 = @(r) 2*pi()*r.*(-3.376e13*r.^4 + 1.812e11*r.^3 - 3.516e8*r.^2 + ...
    3.038e5*r - 51.45);
q77502 = integral(v77502, r1, r22)
%% This section for the 7in 0.75D 0.25O 0.085B FOFC
v1775025 = @(r) 2*pi()*r.*(-6.097e12*r.^4 + 2.965e10*r.^3 - 4.073e7*r.^2 + ...
    1.772e4*r + 39.62).^2;
f1775025 = integral(v1775025, r1, r225);
F775025 = f1775025*rho
v775025 = @(r) 2*pi()*r.*(-6.097e12*r.^4 + 2.965e10*r.^3 - 4.073e7*r.^2 + ...
    1.772e4*r + 39.62);
q775025 = integral(v775025, r1, r225)
%% This section for the 7in 0.75D 0.3O 0.085B FOFC
v177503 = @(r) 2*pi()*r.*(-2.653e12*r.^4 + 1.588e10*r.^3 - 3.234e7*r.^2 + ...
    4.076e4*r + 4.644).^2;
f177503 = integral(v177503, r1, r23);
F77503 = f177503*rho
v77503 = @(r) 2*pi()*r.*(-2.653e12*r.^4 + 1.588e10*r.^3 - 3.234e7*r.^2 + ...
    4.076e4*r + 4.644);
q77503 = integral(v77503, r1, r23)
%% This section for the 7in 0.75D 0.35O 0.085B FOFC
v1775035 = @(r) 2*pi()*r.*(-8.916e11*r.^4 + 4.204e9*r.^3 - 1.115e6*r.^2 - ...
    3492*r + 24.4).^2;
```

```
f1775035 = integral(v1775035, r1, r235);
F775035 = f1775035*rho
v775035 = @(r) 2*pi()*r.*(-8.916e11*r.^4 + 4.204e9*r.^3 - 1.115e6*r.^2 - ...
    3492*r + 24.4);
q775035 = integral(v775035, r1, r235)
%% This section for the 4in 1.1D 0.16O 0.085B FOFC
v1411016 = @(r) 2*pi()*r.*(-3.529e13*r.^4 + 5.843e10*r.^3 + 1.485e8*r.^2 - ...
    3.522e5*r + 238.7).^2;
f1411016 = integral(v1411016, r1, r216);
F411016 = f1411016*rho
v411016 = @(r) 2*pi()*r.*(-3.529e13*r.^4 + 5.843e10*r.^3 + 1.485e8*r.^2 - ...
    3.522e5*r + 238.7);
q411016 = integral(v411016, r1, r216)
%% This section for the 4in 1.1D 0.2O 0.085B FOFC
v141102 = @(r) 2*pi()*r.*(-1.999e13*r.^4 + 8.608e10*r.^3 - 1.11e8*r.^2 + ...
    4.048e4*r + 53.58).^2;
f141102 = integral(v141102, r1, r22);
F41102 = f141102*rho
v41102 = @(r) 2*pi()*r.*(-1.999e13*r.^4 + 8.608e10*r.^3 - 1.11e8*r.^2 + ...
    4.048e4*r + 53.58);
q41102 = integral(v41102, r1, r22)
%% This section for the 4in 1.1D 0.25O 0.085B FOFC
v1411025 = @(r) 2*pi()*r.*(-8.406e12*r.^4 + 5.024e10*r.^3 - 1.059e8*r.^2 + ...
    1.044e5*r - 1.484).^2;
f1411025 = integral(v1411025, r1, r225);
F411025 = f1411025*rho
v411025 = @(r) 2*pi()*r.*(-8.406e12*r.^4 + 5.024e10*r.^3 - 1.059e8*r.^2 + ...
    1.044e5*r - 1.484);
q411025 = integral(v411025, r1, r225)
%% This section for the 4in 1.1D 0.3O 0.085B FOFC
v141103 = @(r) 2*pi()*r.*(-2.553e12*r.^4 + 1.442e10*r.^3 - 2.326e7*r.^2 + ...
    1.696e4*r + 25.37).^2;
f141103 = integral(v141103, r1, r23);
```

```
F41103 = f141103*rho
v41103 = @(r) 2*pi()*r.*(-2.553e12*r.^4 + 1.442e10*r.^3 - 2.326e7*r.^2 + ...
    1.696e4*r + 25.37);
q41103 = integral(v41103, r1, r23)
%% This section for the 4in 1.1D 0.35O 0.085B FOFC
v1411035 = @(r) 2*pi()*r.*(-6.434e11*r.^4 + 1.859e9*r.^3 + 6.869e6*r.^2 - ...
    1.564e4*r + 32.01).^2;
f1411035 = integral(v1411035, r1, r235);
F411035 = f1411035*rho
v411035 = @(r) 2*pi()*r.*(-6.434e11*r.^4 + 1.859e9*r.^3 + 6.869e6*r.^2 - ...
    1.564e4*r + 32.01);
q411035 = integral(v411035, r1, r235)
%% This section for the 4in 0.75D 0.16O 0.085B FOFC
v1475016 = @(r) 2*pi()*r.*(1.038e13*r.^4 - 2.076e11*r.^3 + 7.173e8*r.^2 - ...
    8.82e5*r + 420.1).^2;
f1475016 = integral(v1475016, r1, r216);
F475016 = f1475016*rho
v475016 = @(r) 2*pi()*r.*(1.038e13*r.^4 - 2.076e11*r.^3 + 7.173e8*r.^2 - ...
    8.82e5*r + 420.1);
q475016 = integral(v475016, r1, r216)
%% This section for the 4in 0.75D 0.2O 0.085B FOFC
v147502 = @(r) 2*pi()*r.*(-1.498e13*r.^4 + 5.514e10*r.^3 - 4.621e7*r.^2 - ...
    1.023e4*r + 62.5).^2;
f147502 = integral(v147502, r1, r22);
F47502 = f147502*rho
v47502 = @(r) 2*pi()*r.*(-1.498e13*r.^4 + 5.514e10*r.^3 - 4.621e7*r.^2 - ...
    1.023e4*r + 62.5);
q47502 = integral(v47502, r1, r22)
%% This section for the 4in 0.75D 0.25O 0.085B FOFC
v1475025 = @(r) 2*pi()*r.*(-4.883e12*r.^4 + 2.452e10*r.^3 - 4.181e7*r.^2 + ...
    4.42e4*r + 11.26).^2;
f1475025 = integral(v1475025, r1, r225);
F475025 = f1475025*rho
```

```
v475025 = @(r) 2*pi()*r.*(-4.883e12*r.^4 + 2.452e10*r.^3 - 4.181e7*r.^2 + ...
    4.42e4*r + 11.26);
q475025 = integral(v475025, r1, r225)
%% This section for the 4in 0.75D 0.3O 0.085B FOFC
v147503 = @(r) 2*pi()*r.*(-1.818e12*r.^4 + 7.216e9*r.^3 + 2.321e5*r.^2 - ...
    1.004e4*r + 32.04).^2;
f147503 = integral(v147503, r1, r23);
F47503 = f147503*rho
v47503 = @(r) 2*pi()*r.*(-1.818e12*r.^4 + 7.216e9*r.^3 + 2.321e5*r.^2 - ...
    1.004e4*r + 32.04);
q47503 = integral(v47503, r1, r23)
%% This section for the 4in 0.75D 0.35O 0.085B FOFC
v1475035 = @(r) 2*pi()*r.*(-9.47e11*r.^4 + 4.998e9*r.^3 - 4.808e6*r.^2 + ...
    3018*r + 20.67).^2;
f1475035 = integral(v1475035, r1, r235);
F475035 = f1475035*rho
v475035 = @(r) 2*pi()*r.*(-9.47e11*r.^4 + 4.998e9*r.^3 - 4.808e6*r.^2 + ...
    3018*r + 20.67);
q475035 = integral(v475035, r1, r235)
%% This section for the 4in 0.5D 0.16O 0.085B FOFC
v145016 = @(r) 2*pi()*r.*(1.02e14*r.^4 - 7.094e11*r.^3 + 1.709e9*r.^2 - ...
    1.721e6*r + 675.7).^2;
f145016 = integral(v145016, r1, r216);
F45016 = f145016*rho
v45016 = @(r) 2*pi()*r.*(1.02e14*r.^4 - 7.094e11*r.^3 + 1.709e9*r.^2 - ...
    1.721e6*r + 675.7);
q45016 = integral(v45016, r1, r216)
%% This section for the 4in 0.5D 0.2O 0.085B FOFC
v14502 = @(r) 2*pi()*r.*(-1.902e13*r.^4 + 9.916e10*r.^3 - 1.969e8*r.^2 + ...
    1.964e5*r - 40.08).^2;
f14502 = integral(v14502, r1, r22);
F4502 = f14502*rho
v4502 = @(r) 2*pi()*r.*(-1.238*r.^4 - 6.119*r.^3 - 12.12*r.^2 - 1.185*r + ...
```

```
    54.39);
q4502 = integral(v4502, r1, r22)
%% This section for the 4in 0.5D 0.25O 0.085B FOFC
v145025 = @(r) 2*pi()*r.*(-1.076e13*r.^4 + 7.307e10*r.^3 - 1.862e8*r.^2 + ...
    2.295e5*r - 78.47).^2;
f145025 = integral(v145025, r1, r225);
F45025 = f145025*rho
v45025 = @(r) 2*pi()*r.*(-1.076e13*r.^4 + 7.307e10*r.^3 - 1.862e8*r.^2 + ...
    2.295e5*r - 78.47);
q45025 = integral(v45025, r1, r225)
%% This section to compare/compile the information

L7D11 = [Ff16f, Ff2, Ff25, Ff3, Ff35];
L7D75 = [F775016, F77502, F775025, F77503, F775035];
L7D5 = [FL16, FL2, FL25, 0, 0];
L7D5s = [FL16, FL2, FL25];
L4D11 = [F411016, F41102, F411025, F41103, F411035];
L4D75 = [F475016, F47502, F475025, F47503, F475035];
L4D5 = [F45016, F4502, F45025, 0, 0];
L4D5s = [F45016, F4502, F45025];
orificeL = [0.16 0.2 0.25 0.3 0.35];
orificeS = [0.16 0.2 0.25];

QL7D11 = [qf16f, qf2, qf25, qf3, qf35];
QL7D75 = [q775016, q77502, q775025, q77503, q775035];
QL7D5 = [qL16, qL2, qL25, 0, 0];
QL4D11 = [q411016, q41102, q411025, q41103, q411035];
QL4D75 = [q475016, q47502, q475025, q47503, q475035];
QL4D5 = [q45016, q4502, q45025, 0, 0];

ScaleUpForce = [Ff16f, Ff2, Ff25, Ff3, Ff35, Ff4, Ff45, Ff5];
ScaleUpForceEnglish = ScaleUpForce/4.4482216;

```

```
lengthComparisonTable = [transpose(L7D11) transpose(L7D75) transpose(L7D5) ...
    transpose(L4D11) transpose(L4D75) transpose(L4D5)];
lengthComparisonTableFlow = [transpose(QL7D11) transpose(QL7D75) ...
    transpose(QL7D5) transpose(QL4D11) transpose(QL4D75) transpose(QL4D5)];

lengthComparisonTableEnglish = [transpose(L7D11) transpose(L7D75) ...
    transpose(L7D5) transpose(L4D11) transpose(L4D75) ...
    transpose(L4D5)]/4.4482216;
lengthComparisonTableFlowEnglish = [transpose(QL7D11) transpose(QL7D75) ...
    transpose(QL7D5) transpose(QL4D11) transpose(QL4D75) ...
    transpose(QL4D5)]*15850.32;
```

This script provided the force values for all scenarios as well as a section for comparison of the force and flows.

B.2 Dynamic Modeling

Next, the forces calculated with $Force\_Balance\_Orifice\_Size\_Optimization\_1mm$ were used in conjunction with the dynamic model. The functionosc_motion was used to store the nonlinear forcing functions based on the input force. This can be seen below.

```
function xdot = osc_motion(ti,y)
global m Fmax kw n cw g
ts = ti*n+1;
x1 = .001*0.95; %This is to account for the fact that some force is still ...
    exerted when the shaker is near, but not at, FOFC position
Fric = m*g*0.0425; %.024 is likely the amount of friction to be ...
    experienced due to ball bearings

tee = ti;

if y(1,1) < -0.001 + x1 && y(1,1) < 0 && y(2,1) >= 0
     F_jet = Fmax;
```

```
elseif y(1,1) > 0.001 - x1 && y(1,1) > 0 && y(2,1) <= 0
    F_jet = -Fmax;
else
    F_jet = 0;
end


if y(1,1) < -0.00105
    F_wall = -kw*(y(1,1) + 0.00105) - cw*y(2,1);
elseif y(1,1) > 0.00105
    F_wall = -kw*(y(1,1) - 0.00105) - cw*y(2,1);
else
    F_wall = 0;
end

if y(2,1) > 0
    F_fric = -1*Fric;
elseif y(2,1) < 0
    F_fric = Fric;
else
    F_fric = 0;
end


F = F_jet + F_wall + F_fric;

xdot = zeros(2,1);
xdot(2,1) = F/m;
xdot(1,1) = y(2,1);
```

Next, *osc_motion* was used as part of the larger model *osc_model* (shown below), which is the script where the force and mass inputs were included. Then *ode*45 was used to solve the nonlinear differential equation in *osc_motion*.

```
global m Fmax kw n cw g
num = 5;
m = 28;
g = 9.81;
Fmax = Ff16f;
w = 20*2*pi();
kw = 100000000;
zeta = 0.005;
cw = zeta*sqrt(kw*m);
ks = (20*pi()*2)^2*m*0.9;
n = 5000;
xg = 8;
tspan = 0:1/n:(xg-1/n);
x10 = -0.001;
x20 = 0;
x0 = [x10; x20];
E_bt = 200e9; %if ball transfer is A36
nu_bt = 0.26; %if ball transfer is A36
R_bt = 0.004318/2;
rho_bt = 7800;
E_wall = 200e9;
nu_wall = 0.26;
E_star_i = (E_bt/(1-nu_bt^2))^(-1) + (E_wall/(1-nu_wall^2))^(-1);
E_star = 1/E_star_i;

Fs = n/xg;
f = Fs*(0:(n/2))/n;

[t,x] = ode45('osc_motion', tspan, x0);
fouri = fft(x(:,1));
P2 = abs(fouri/n);
P1 = P2(1:n/2+1);
P1(2:end-1) = 2*P1(2:end-1);
```

```
alpha = find(P1 == max(P1));
osc_freq = f(alpha);

%% This section calculates the order of magnitude of the acoustic and ...
   collision effects.
%The model used does not account for these effects since they are
%negligible
oom_coll = 10^ceil(log10(E_star*max(x(:,2))^3*(R_bt)^3/m)^(1/5));
oom_mat = 10^ceil(log10((E_bt/rho_bt)^(0.5)));
if oom_coll >= oom_mat/10
    warning('This problem has a non-negligible acoustic effect that is not ...
       being accounted for. Consider a more rigorous solution which would ...
       be able to account for this.');
end

%% Graphing

%This is to show where the walls are in relation to the motion of the
%shaker
for i = 1:length(tspan)
    const_pos(i) = 0.001;
    const_neg(i) = -0.001;
end


% subplot(2,1,1)
figure
plot(tspan, x(:,1), 'b', tspan, const_pos, 'r', tspan, const_neg, 'r')
% title('Position vs Time')
ylabel('Position (m)')
xlabel('Time (s)')
ylim([-.002, .002])
xlim([0, 4])
```

```
set(findall(gca, 'Type', 'Line'),'LineWidth',2);

% subplot(2,1,2)
% plot(tspan, x(:,2), 'b')
% title('Velocity vs Time')
% ylabel('Velocity (m/s)')
% xlabel('Time (s)')
% xlim([0, 8])
% set(findall(gca, 'Type', 'Line'),'LineWidth',2);

% since gc is so small, the velocity after bouncing off the wall is 0.9994
% times the velocity right before hitting the wall. Thus it can be
% determined that the losses due to material dissipation are negligible.



% subplot(2,1,2)
figure
plot(f,P1)
%title('Single-Sided Amplitude Spectrum of X(t)')
xlim([0, 100]);
xlabel('f (Hz)')
ylabel('|P1(f)|')
```

B.3 Scaling Up

Finally, a model was generated to determine the amount of mass that could be shaken based on orifice size and wall stiffness. This script, $Orifice\_Optimization$ (shown below) was used on conjunction with osc_motion, $ode45$, and the FFT function.

```
global m Fmax kw n cw g
num = 5;
```

```
m = 20;
g = 9.81;
w = 20*2*pi();
kw = 6.5e5;
zeta = 0.005;
cw = zeta*sqrt(kw*m);
ks = (20*pi()*2)^2*m*0.9;
n = 5000;
xg = 8;
tspan = 0:1/n:(xg-1/n);
x10 = -0.001;
x20 = 0;
x0 = [x10; x20];
E_bt = 200e9; %if ball transfer is A36
nu_bt = 0.26; %if ball transfer is A36
R_bt = 0.004318/2;
rho_bt = 7800;
E_wall = 200e9;
nu_wall = 0.26;
E_star_i = (E_bt/(1-nu_bt^2))^(-1) + (E_wall/(1-nu_wall^2))^(-1);
E_star = 1/E_star_i;

Fs = n/xg;
f = Fs*(0:(n/2))/n;
wn = 20*2*pi; %natural frequency for the shaker should be equal to the ...
    desired vibration frequency

orifice = [0.16 0.2 0.25 0.3 0.35 0.4 0.45 0.5];
mm = 25;
K = logspace(5, 8, mm);
M = ones(mm,8);
osc_freq = 31*ones(mm,8);
Force = [Ff16 Ff2 Ff25 Ff3 Ff35 Ff4 Ff45 Ff5];
```

```
for pp = 1:8
    Fmax = 2*Force(pp);
    pp
    for ii = 1:mm
        if ii == 1
            M(ii,pp) = 1;
        else
            M(ii,pp) = M(ii-1,pp);
        end
        while osc_freq(ii,pp) > 21.5 || osc_freq(ii,pp) < 18.5
            kw = K(ii);
            m = M(ii,pp);
            [t,x] = ode45('osc_motion', tspan, x0);
            fouri = fft(x(length(x(:,1))/2:end,1));
            P2 = abs(fouri/n);
            P1 = P2(1:n/2+1);
            P1(2:end-1) = 2*P1(2:end-1);
            alpha = find(P1 == max(P1));
            osc_freq(ii,pp) = f(alpha);
                 if osc_freq(ii,pp) >= 30
                    M(ii,pp) = M(ii,pp) + 250/(K(ii)^0.5);
                elseif osc_freq(ii,pp) < 30 && osc_freq(ii,pp) >= 25.5
                    M(ii,pp) = M(ii,pp) + 150/(K(ii)^0.5);
                elseif osc_freq(ii,pp) < 25.5 && osc_freq(ii,pp) >= 23
                    M(ii,pp) = M(ii,pp) + 100/(K(ii)^0.5);
                elseif osc_freq(ii,pp) < 23 && osc_freq(ii,pp) >= 21.5
                    M(ii,pp) = M(ii,pp) + 25/(K(ii)^0.5);
                elseif osc_freq(ii,pp) <= 10
                    M(ii,pp) = M(ii,pp) - 10/(K(ii)^0.5);
                elseif osc_freq(ii,pp) > 10 && osc_freq(ii,pp) <= 14.5
                    M(ii,pp) = M(ii,pp) - 0.1/(K(ii)^0.5);
                elseif osc_freq(ii,pp) > 14.5 && osc_freq(ii,pp) <= 18.5
                    M(ii,pp) = M(ii,pp) - 0.01/(K(ii)^0.5);
```

```
                    end
                M(:,pp);
                osc_freq(:,pp);
                pp
                ii
            end
        end
    end
```

This was then plotted with the script $Orifice\_Optimization\_Grapher$ as shown below.

```
%M = zeros(20,7);
K = logspace(5,8,25);
wn = 20*2*pi();
M_ideal = K./(wn^2);
color = ['b' 'r' 'k' 'g' 'y' 'm' 'c' 'b-.'];

for ii = 1:8
    semilogx(K,M(:,ii), color(ii), 'LineWidth', 2)
    hold on
end
%plot(K, M_ideal)
xlabel('Stiffness (N/m)')
ylabel('Mass shaken (kg)')
legend('0.16in orifice', '0.2in orifice', '0.25in orifice', '0.3in ...
    orifice', '0.35in orifice', '0.4in orifice', '0.45in orifice', '0.5in ...
    orifice')
```